Next-Cycle Optimal Dilute Combustion Control via Online Learning of Cycle-to-Cycle Variability using Kernel Density Estimators

Bryan P. Maldonado, *Member, IEEE,* Brian C. Kaul, Catherine D. Schuman, *Senior Member, IEEE,* Steven R. Young, *Member, IEEE,* and J. Parker Mitchell, *Member, IEEE*

***Abstract*—Dilute combustion using exhaust gas recirculation (EGR) presents a cost-effective method for increasing the efficiency of spark-ignition engines. However, the maximum amount of EGR that can be used at a given condition is limited by a rapid increment of cycle-to-cycle variability (CCV). This study describes a methodology to design a model-based stochastic optimal controller to adjust the cycle-to-cycle fuel injection quantity in order to reduce CCV and further extend the dilute limit. Given the complexity and chaotic nature of combustion events, the controller was enhanced with online learning in order to identify the statistical properties of combustion efficiency, which are needed to generate predictions for next-cycle events. This study showed that a kernel density estimator (KDE) can be used to learn the combustion properties in real-time and can be incorporated into the feedback policy in order to calculate the optimal control command. Experimental results suggested that the dilute limit can be extended from 18.5% to 21% EGR fraction at an operating condition relevant for highway cruising. Additionally, the proposed controller can achieve a large CCV reduction with less fuel enrichment compared to previous methods, overall contributing to an increase in 0.2% indicated fuel conversion efficiency.**

***Index Terms*—Internal combustion engines, Stochastic systems, Statistical learning, Optimal control, Kernel density estimation.**

I. Introduction

INCREASINGLY stringent regulations in greenhouse gas emissions require a continuous improvement of fuel efficiency in the transportation sector, whose energy consumption depends mostly on fossil fuels. The U.S. Energy Information Administration (EIA) in its 2021 Annual Energy Outlook [1] indicated that light-duty vehicles consumed as much as 75% of the total energy used by the transportation sector in 2019, with projections suggesting a modest decrease to 70% share by 2050. Currently, spark-ignition (SI) internal combustion engines dominate the light-duty vehicle market, corresponding to a 98% market share in 2020 (including hybrid powertrains). Even though battery-electric and plug-in hybrid electric vehicles have steadily gained market penetration, the EIA forecasts that SI gasoline engines will remain relevant through 2050 by powering over 87% of passenger vehicles. Medium- and heavy-duty vehicles will remain dependent on internal combustion engines for the foreseeable future due to their heavier duty cycles, with SI engines offering the potential for efficiency and emissions improvement, particularly in the medium-duty sector. Consequently, increasing the efficiency of SI engines can substantially improve the fuel economy of the light-duty and the medium-duty sector in the longer term.

Dilute combustion by means of exhaust gas recirculation (EGR) is a technologically proven and cost-effective way to reduce fuel consumption on a broad scale. The efficiency gain comes primarily at part load via improved gas properties, decreased throttling losses, and decreased heat losses [2]. However, EGR affects the combustion kinetics and increases the sensitivity of ignition with respect to in-cylinder composition. Combustion stability is then limited either by poor flame initiation (misfires) [3], [4] or propagation (partial burns) [5], which increase the cycle-to-cycle variability (CCV) even if the spark advance is optimized. These issues may become more pronounced for future medium-duty SI gaseous and low-carbon fuels with reduced flame speeds. Even though misfire detection is a required component of on-board diagnostics, accurate prediction and avoidance of such events remains an open problem. In particular, misfire avoidance is critical to maintain adequate drivability without excessive vibrations [6]. Therefore, a successful dilute combustion management will maximize the levels of EGR while avoiding misfires and partial burns in order to guarantee maximum engine efficiency, improved emissions, and comply with drivability standards.

The controllability of dilute combustion is directly tied to the deterministic patterns of combustion CCV. In the case of dilute SI combustion, the deterministic behavior of CCV is attributed to a nonlinear dependence of flame initiation and flame speed on composition, with feedforward communication between cycles due to residual gas composition [7]. The quantity and composition of residual gas on a given cycle directly impact the subsequent combustion event, serving as the mechanism for deterministic coupling between cycles. The presence of such determinism implies that active control can reduce instabilities in combustion at the dilute limit,

B. P. Maldonado and B. C. Kaul are with the Buildings and Transportation Science Division, Oak Ridge National Laboratory, Oak Ridge, TN 37830 USA (e-mail: maldonadopbp@ornl.gov; kaulbc@ornl.gov).

C. D. Schuman, S. R. Young, and J. P. Mitchell are with the Computer Science and Mathematics Division, Oak Ridge National Laboratory, Oak Ridge, TN 37830 USA (e-mail: schumancd@ornl.gov; youngsr@ornl.gov; mitchelljp1@ornl.gov).

This manuscript has been authored by UT-Battelle, LLC under Contract No. DE-AC05-00OR22725 with the U.S. Department of Energy. The United States Government retains and the publisher, by accepting the article for publication, acknowledges that the United States Government retains a non-exclusive, paid-up, irrevocable, world-wide license to publish or reproduce the published form of this manuscript, or allow others to do so, for United States Government purposes. The Department of Energy will provide public access to these results of federally sponsored research in accordance with the DOE Public Access Plan (http://energy.gov/downloads/doe-public-access-plan).

and a proof of concept has been demonstrated using simple proportional feedback control [8]. Under nominal conditions, combustion events are considered uncorrelated and CCV has been modeled using a Gaussian random process [9], [10]. Past the dilute limit, however, combustion CCV exhibits deterministic features with stochastic variations [11]–[15].

The cycle-to-cycle determinism could be used to mitigate undesired combustion events by two possible engine actuators: spark advance and fuel injection quantity [16]. In general, studies regarding spark advance control are limited to tracking optimal combustion phasing either using model-based control techniques [17]–[19] or artificial intelligence methods [20]–[22]. Previous research has designed a controller to limit the misfire occurrence rate at the dilute limit [23]. However, misfires were assumed to be random and the deterministic effect of residual gas was not considered. Another study used a coordinated control of spark advance and EGR valve in order to identify and avoid the dilute limit during engine transients [24]. This study, however, seeks not only to identify but also to extend the dilute limit using fuel injection control. Although Xu *et al.* demonstrated a successful coordinated control of spark advance and fuel quantity for increased thermal efficiency during lean combustion [25], the optimization was performed model-free. In contrast, the proposed study considered a model-based control approach where the physics of combustion tie the fuel quantity directly to the energy released during each cycle, making it possible to develop simple models that depend on residual gas effects [26]. Therefore, the model-based strategy presented in this paper is limited to fuel quantity control and will not adjust the spark advance.

During conditions past the dilute limit, the propensity of partial burns and misfires can be significantly reduced by enriching the air-fuel charge due to the increase in laminar flame speed [27]. The flame propagation, from the kernel formation to its development into a turbulent flame, depends on the laminar flame speed. Therefore, a higher laminar flame speed can cancel the negative effect EGR has on the combustion kinetics. Moreover, it has been shown experimentally that small perturbations in fuel quantity, ranging from 0.5% to 2% additional fuel, can produce detectable changes in combustion CCV [28]. This suggests that a next-cycle predictive control of fuel injection quantity could attempt to enrich the charge only when a low-energy event is predicted. Even though stoichiometric operation with EGR allows for improved efficiency while maintaining compatibility with the TWC to control emissions, the objective of this study is to investigate the theoretical properties of the feedback policy proposed to reduce CCV. Thus, during closed-loop, the feedback from the exhaust oxygen sensor was ignored and net enrichment was allowed to quantify the effectiveness of the controller.

The stochastic optimal control problem was formulated using a cost function that penalized high combustion CCV as well as deviations from stoichiometric combustion. Combining the cost function with a model-based design, it was demonstrated that knowledge of the first and second moments of the cycle-to-cycle combustion efficiency suffice to predict the next-cycle combustion behavior. The statistical properties were estimated using an online learning algorithm based on the kernel density estimator. This paper is a continuation of a previous simulation study performed by the authors [29] and includes a detailed analysis of the control design together with closed-loop experiments to validate the theoretical results. Additionally, a comparison was made against a previously designed neural network-based controller, showing that the proposed feedback policy is more effective at using the cycle-to-cycle deterministic combustion dynamics.

TABLE I
ENGINE CHARACTERISTICS AND OPERATING CONDITIONS

Displaced Volume	500 cm^3
Bore × Stroke	86 mm × 86 mm
Connecting Rod	145 mm
Compression Ratio	9.2 : 1
Intake Valve Opening (IVO)	$-357°$aTDC
Intake Valve Closing (IVC)	$-100°$aTDC
Exhaust Valve Opening (EVO)	$150°$aTDC
Exhaust Valve Closing (EVC)	$357°$aTDC
Engine Speed	1480 rpm
Start of Injection	$-280°$aTDC
Indicated Load (IMEP)	7.8 bar
Coolant & Oil Temperature	$70°$C
EGR Cooler Temperature	$50°$C
Intake Manifold Temperature	$35°$C

The remaining sections are organized as follows. Section II describes the experimental setup. Section III shows the characteristic of CCV. Section IV describes the control-oriented model, as well as the online state estimation algorithm. Section V defines the stochastic optimal control problem. Section VI shows the online learning algorithm used for next-cycle predictive control. Finally, Section VII presents the experimental results that show the extension of the dilute limit.

II. EXPERIMENTAL SETUP

The data used for this study were collected from a single-cylinder version of a 2 L GM Ecotec LNF engine. Table I summarizes the combustion chamber geometry and the operating conditions considered for this work. Even though the experiments were conducted in a single-cylinder engine, where cylinder-to-cylinder disturbances on EGR and residual gas fraction cannot be captured, other studies have shown the feasibility of 1) modeling of cylinder-to-cylinder correlation effects in CCV [30], 2) individual cylinder charge estimation [31], and 3) cylinder-to-cylinder CCV control using spark advance [32]. Therefore, it is expected that the results presented in this study can be replicated in a multi-cylinder engine. Consideration of cylinder-to-cylinder interactions and the complex dynamics involved is follow-on work that would be needed, but single-cylinder effectiveness must be demonstrated first before it can be extended to the more complex multi-cylinder case.

The spark-ignition direct-injection experimental engine was equipped with variable cam timing and an external, cooled, low-pressure EGR system. The engine speed was kept constant using an engine dynamometer. Airflow was kept constant at a medium load for all experimental conditions using an Alicat mass flow controller. A wide-band exhaust oxygen sensor was utilized to adjust the feedforward fuel quantity

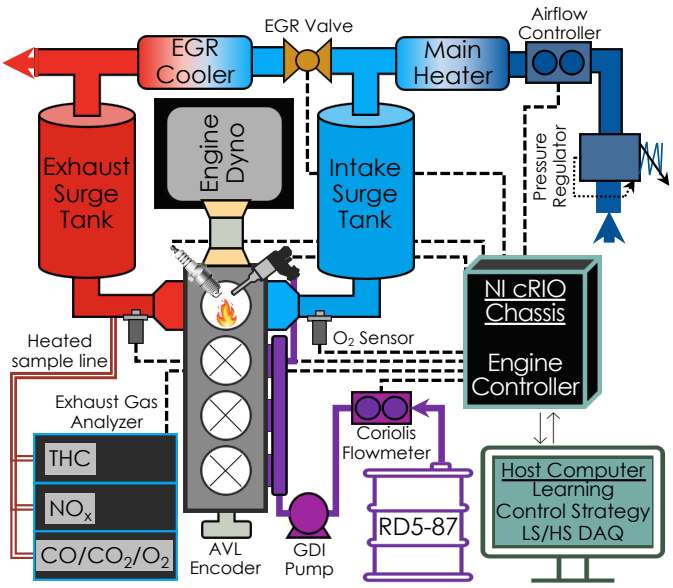

Fig. 1. Experimental setup with rapid prototyping ECU and instrumentation.

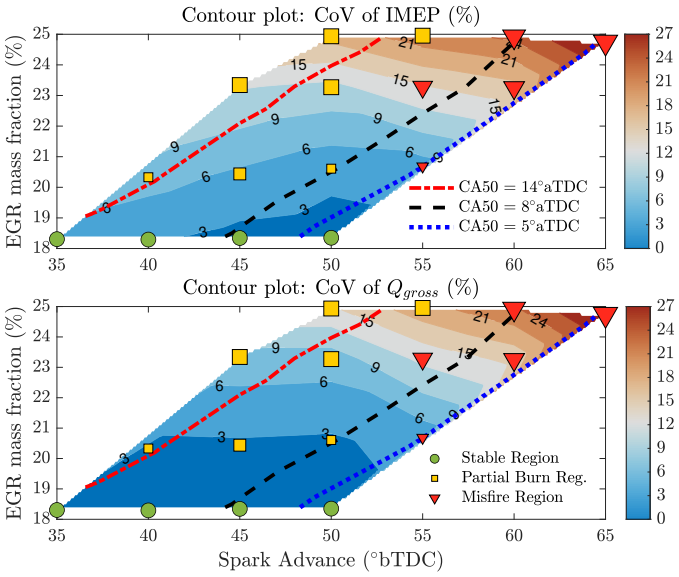

Fig. 2. CoV values for IMEP (top) and Q_{gross} (bottom) during an open-loop spark/EGR sweep. Markers indicate operating conditions considered with marker size indicating relative number of incomplete combustion events. Dash-dotted, dashed, and dotted lines represent different CA50 locations.

to maintain a stoichiometric charge during open-loop. The start of injection was kept fixed at -280°aTDC during open- and closed-loop operation. The early timing was chosen to promote a homogeneous air-fuel mixture and avoid possible fuel stratification that could affect the CCV. The cam timing remained fixed and was chosen to avoid valve overlap. The EGR molar fraction in the intake manifold was calculated using intake oxygen measurements. The EGR mass fraction was calculated using the mole fraction and the molecular weights of air and EGR. In-cylinder pressure was measured using a Kistler 6125C flush-mounted piezoelectric pressure transducer. Research-grade E10 gasoline known as RD5-87, which was designed to be representative of regular-grade market gasoline, was utilized. In addition, exhaust gas analyzers were utilized to measure the concentrations of O_2, CO, CO_2, NO_x, and total hydrocarbons (THC). Emissions data were mainly used to estimate the average combustion efficiency at each condition.

An open LabVIEW-based engine control unit (ECU) implemented on a National Instruments CompactRIO (NI cRIO) hardware was used for the low-level engine control. The high-level controller, data processing, and data acquisition, however, were implemented in a host computer using an in-house LabVIEW-based Oak Ridge Combustion Analysis System (ORCAS). Even though the ORCAS calculations, learning algorithm, and optimal control policy calculations took no more than 2 ms in the host computer, analog communications with the NI cRIO chassis limited this study to a maximum engine speed of 1480 rpm. Nonetheless, higher engine speeds can be achieved if all calculations were to be done onboard and integrated into the ECU without communication overhead, as previously done by Luo *et al.* [33]. The engine architecture and the rapid prototyping ECU are depicted in Fig. 1.

III. Combustion Variability at the Dilute Limit

The engine speed and load were kept constant at 1480 rpm and 7.8 bar indicated mean effective pressure (IMEP), respectively. This condition corresponds to a typical mid-load cruising operation where EGR contributes to an increase in engine efficiency [2]. The operating condition was informed by the advanced combustion and emission control (ACEC) tech team [34]. While down-speeding to 1480 rpm was required due to communication latencies, the power level was fixed to the ACEC Roadmap recommendation. A steady-state speed and load operation was considered exclusively in this study for two main reasons. First, this is initial proof-of-concept research, and demonstrating effectiveness in steady-state operation was deemed a reasonable step before extending to transient operation. Second, since this is a cycle-resolved control strategy, it is inherently faster than load transients which are mainly driven by engine breathing dynamics. Moreover, other studies have shown that the dynamic behavior observed at the dilute or lean limits are similar for a wide variety of engine loads [35]. Therefore, as long it is paired with a good estimator of in-cylinder mass and composition, the methodology should remain effective at different loads and during load transients.

Figure 2 shows the sweep in spark advance and EGR fraction performed around the optimal combustion phasing and passed the dilute limit to explore different CCV characteristics [14]. At each spark/EGR combination, 3000 consecutive engine cycles were recorded. The combustion phasing was quantified by the crank angle location for 50% mass fuel burned (CA50). For a fixed EGR level, the spark advance was adjusted such that CA50 ranged from 5 to 15°aTDC. The EGR levels were increased up to 25%, where high CCV was detected. The CCV is typically quantified by the coefficient of variation (CoV) of IMEP. In general, industry standards limit the CoV of IMEP to a maximum of 3% based on the levels of noise, vibration, and harshness experienced by the driver. For this operating condition, the dilute limit was reached at approximately 18.5% EGR fraction at optimal spark advance.

For all the spark/EGR combinations, Fig. 2 shows the contour plots of the values for CoV of IMEP (top) and the CoV of gross heat release Q_{gross} (bottom). The x-axis corresponds to the spark command while the y-axis corresponds to the average EGR fraction. All operating conditions had a similar standard deviation for the EGR measurements around 0.57%. As expected, the CoV of IMEP increases rapidly as EGR increases past the dilute limit, mainly due to partial burns and misfires. Three distinct combustion regions can be identified in Fig. 2 depending on the dominance of misfires ($Q_{\text{gross}} \leq 0$) or partial burns. Here, partial burns were defined as combustion events with $Q_{\text{gross}} > 0$ but energy release lower than 75% of nominal. The proposed regions can be defined as follows:

1) Stable Region (◯ markers): No misfires or partial burns detected during 3000 engine cycles.
2) Partial Burn Region (□ markers): Number of partial burns exceed the number of misfires observed.
3) Misfire Region (▽ markers): Misfires dominate the instabilities observed.

In addition, the markers representing the partial burn and misfire regions have been scaled to represent the relative number of low-energy events in each region. The number of misfire events increases with spark advance while the number of partial burns increases at retarded combustion phasing. Even though the spark is typically calibrated for optimal combustion phasing, aiming for CA50 = 8°aTDC (depicted by the black dashed line) [36], [37], the proposed controller was also tested at retarded (red dash-dotted line) and advanced (blue dotted line) combustion phasings. In particular, the solution of the next-cycle control problem at partial-burn-dominated conditions could be applied to CCV reduction during cold starts where retarded combustion is used to increase the gas enthalpy and warmup the aftertreatment system [38]–[40].

The values of the gross heat release are not only important for classifying partial burns but were also used as proxy for CCV control. Given the structure of the model, Q_{gross} was introduced into the cost function in order to penalize high CCV. The bottom plot of Fig. 2 indicates that the CoV values of IMEP and Q_{gross} are in close agreement at advanced combustion phasing. At retarded combustion phasing, however, the CoV of IMEP increases more rapidly than the CoV of Q_{gross} as EGR levels increase. This occurs because IMEP is more sensitive to phasing than the gross heat release. Since combustion phasing is correlated with spark advance, the top plot of Fig. 2 shows that the CoV of IMEP increases from 18% EGR up to 22% EGR as spark advance retards. This is not the case for the bottom plot, where the CoV of Q_{gross} does not change significantly as the spark advance changes. Given that the proposed model predicts Q_{gross} and not IMEP, centralized coordination of spark advance and fuel quantity was not considered for the proposed control strategy. Alternatively, a decentralized control strategy could be adopted where the proposed controller adjusts the fuel quantity and another controller adjusts the spark advance to optimize combustion and reduce CCV. Finally, since Q_{gross} was used as proxy for CCV, it is necessary to determine if such a variable exhibits the deterministic behavior needed for next-cycle control.

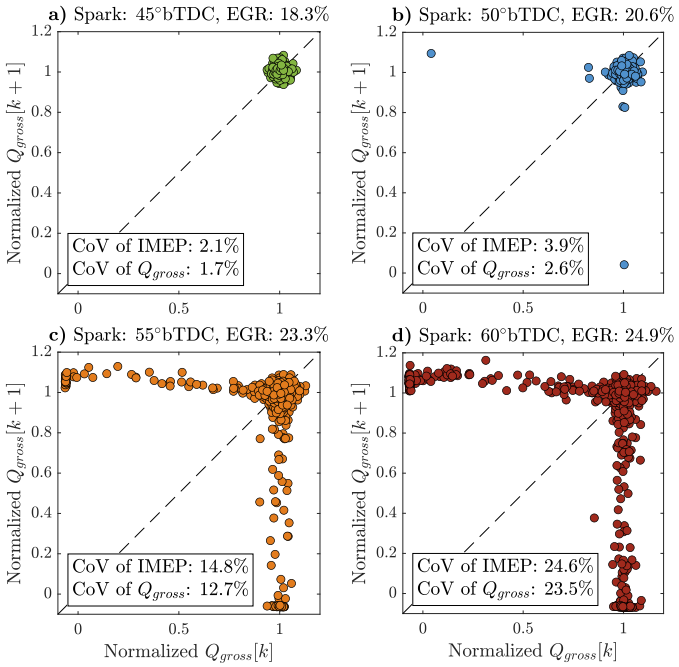

Fig. 3. Return maps of 3000 cycles of normalized Q_{gross} at different levels of EGR and spark advance calibrated for optimal combustion phasing.

A. Deterministic Component of Cycle-to-Cycle Variability

Figure 3 shows the return maps of the normalized Q_{gross} for the four points at spark advance calibrated for optimal combustion phasing. Right at the dilute limit, at 18.3% EGR fraction (subplot a), the return map shows a dispersed but compact pattern centered at the nominal value, which reflects the pure randomness of the combustion CCV. Slightly past the dilute limit, at 20.6% EGR fraction (subplot b), the return map shows a limited number of low-energy events. At 23.3% EGR fraction (subplot c), the sensitivity of the flame kernel development increases, and the return map forms "arms" that extend all the way to the misfire zone ($Q_{\text{gross}} < 0$) increasing the occurrence of low-energy cycles. Finally, at 24.9% EGR fraction (subplot d), CCV has been significant exacerbated by the high number of partial burns and misfires (256) detected in 3000 cycles. This unstable combustion behavior at highly lean and EGR-diluted conditions was analyzed initially by Quader [41]. Note that the return maps for conditions over the misfire limit (23.3% and 24.9% EGR fraction) exhibit an asymmetric shape with respect to the $x = y$ diagonal. This suggests some level of prior-cycle correlation. As previously observed by Kaul *et al.* [11], combustion cycles with significantly low energy release leave a substantial amount of residual oxygen and fuel remaining to be used during the next cycle. Hence, such events are followed by cycles with high energy release. This deterministic behavior was captured by a linear time-varying system used for model-based control.

IV. Control-Oriented Model

The control-oriented model used for control design is a generalization of the physics-based approach for lean combustion presented by Daw *et al.* [7]. The dynamic coupling between

TABLE II
SPECTRAL DECOMPOSITION OF SYSTEM MATRIX AND CONTROLLABILITY MATRIX FOR ORIGINAL AND REDUCED-ORDER SYSTEMS

Matrix	Rank	Eigenvalues	Eigenvectors
$\widetilde{A}_k$	3	$X_{\text{res}}[k](1-\eta_c[k])$ $X_{\text{res}}[k]$ $X_{\text{res}}[k]$	$\begin{bmatrix}1\\ \text{AFR}_\text{s}\\ -(1+\text{AFR}_\text{s})\end{bmatrix}, \begin{bmatrix}0\\1\\0\end{bmatrix}, \begin{bmatrix}0\\0\\1\end{bmatrix}$
$\widetilde{\mathcal{C}}_k$	2	1 0 $-X_k\eta_k\left[\text{AFR}_\text{s}-X_k(2-\eta_k)(1+\text{AFR}_\text{s})\right]$	$\begin{bmatrix}1\\0\\0\end{bmatrix}, \begin{bmatrix}X_k^2(1-\eta_k)\\-X_k(2-\eta_k)\\1\end{bmatrix}, \begin{bmatrix}-\dfrac{X_k(1-\eta_k)\left[\text{AFR}_\text{s}-X_k(1-\eta_k)(1+\text{AFR}_\text{s})\right]}{1+X_k\eta_k\left[\text{AFR}_\text{s}-X_k(2-\eta_k)(1+\text{AFR}_\text{s})\right]}\\ \text{AFR}_\text{s}\\ -(1+\text{AFR}_\text{s})\end{bmatrix}$
A_k	2	$X_{\text{res}}[k](1-\eta_c[k])$ $X_{\text{res}}[k]$	$\begin{bmatrix}-1\\1\end{bmatrix}, \begin{bmatrix}0\\1\end{bmatrix}$
$\mathcal{C}_k$	2	1 $X_{\text{res}}[k]\eta_c[k]$	$\begin{bmatrix}1\\0\end{bmatrix}, \begin{bmatrix}-X_{\text{res}}[k](1-\eta_c[k])\\(1-X_{\text{res}}[k]\eta_c[k])\end{bmatrix}$

Note: $X_k = X_{\text{res}}[k]$, $\eta_k = \eta_c[k]$

combustion cycles is through the carryover of residual gas from the previous cycle to the next and can be described by the following discrete-time linear time-varying (LTV) system:

$$\begin{bmatrix}M_{\text{fuel}}\\M_{\text{air}}\\M_{\text{inert}}\end{bmatrix}_{k+1} = \underbrace{X_{\text{res}}[k]\begin{bmatrix}1-\eta_c[k] & 0 & 0\\ -\text{AFR}_\text{s}\eta_c[k] & 1 & 0\\ (1+\text{AFR}_\text{s})\eta_c[k] & 0 & 1\end{bmatrix}}_{\widetilde{A}_k}\begin{bmatrix}M_{\text{fuel}}\\M_{\text{air}}\\M_{\text{inert}}\end{bmatrix}_k + \underbrace{\begin{bmatrix}1\\0\\0\end{bmatrix}}_{\widetilde{B}} m_{\text{fuel,in}}[k] + \underbrace{\begin{bmatrix}0\\1\\\dfrac{X_{\text{EGR}}}{1-X_{\text{EGR}}}\end{bmatrix}}_{\widetilde{E}} m_{\text{air,in}}\,. \tag{1}$$

Here, $M_{\text{fuel}}[k]$, $M_{\text{air}}[k]$, and $M_{\text{inert}}[k]$ correspond to the total in-cylinder mass of fuel, air, and inert gases, respectively. The fresh charge is comprised of the injected fuel quantity command $u_k = m_{\text{fuel,in}}[k]$, the fresh air $m_{\text{air,in}}$, and the EGR fraction X_{EGR}. Here, the cycle $k+1$ starts at intake valve closing (IVC), which is affected by the fuel injection u_k occurring before IVC. In addition, the model assumes that X_{EGR} and $m_{\text{air,in}}$ remain constant since they would not vary instantaneously on a cycle-to-cycle basis. The parameters of the matrix $\widetilde{A}_k$ determine the amount and composition of the residual mass. The stoichiometric air-to-fuel ratio $\text{AFR}_\text{s} = 14.6$ was considered as a constant property of the fuel. The combustion efficiency $\eta_c[k]$ and the residual gas fraction $X_{\text{res}}[k]$, however, were considered as stochastic variables indexed by k which introduce combustion CCV in the model. Although this model is advantageous at capturing the chaotic combustion dynamics, it fails at including the spark advance as a control input. This is due to the simplicity of the model that only considers the effect of the total in-cylinder mass on combustion and neglects the influence of start of injection or start of combustion.

The system matrix $\widetilde{A}_k$ is lower triangular with nonzero diagonal elements. Its spectral decomposition can be found in Table II. The physical interpretation of the residual gas fraction and the combustion efficiency ($0 < X_{\text{res}}, \eta_c < 1$) guarantees that $\widetilde{A}_k$ is Schur stable. In other words, all eigenvalues of $\widetilde{A}_k$ have norm strictly less than one, rendering the system stable. Note, however, that the subspace spanned by the states $\{M_{\text{air}}, M_{\text{inert}}\}$ shares the same eigenvalue. Consider now the cycle-to-cycle controllability matrix defined as:

$$\widetilde{\mathcal{C}}_k = \begin{bmatrix}\widetilde{B} & \widetilde{A}_k\widetilde{B} & \widetilde{A}_k^2\widetilde{B}\end{bmatrix}. \tag{2}$$

Table II shows that the matrix $\widetilde{\mathcal{C}}_k$ is singular since it has a zero eigenvalue. This implies that there are uncontrollable modes in the state space. Even though all modes are stable, this motivates the search for a reduced-order model that is fully controllable. Consider the following linear transformation:

$$L\colon \mathbb{R}^3 \to \mathbb{R}^2 \text{ such that } \begin{bmatrix}M_{\text{fuel}}\\M_{\text{gas}}\end{bmatrix} = \begin{bmatrix}1 & 0 & 0\\0 & 1 & 1\end{bmatrix}\begin{bmatrix}M_{\text{fuel}}\\M_{\text{air}}\\M_{\text{inert}}\end{bmatrix} \tag{3}$$

where M_{gas} represents the total in-cylinder mass of air and inert gases combined. Based on the previous remarks, this mapping was chosen to reduce the dimensionality of the space spanned by $\{M_{\text{air}}, M_{\text{inert}}\}$. The new matrices for the dynamic system can be calculated as $A_k = L\widetilde{A}_kL_R^{-1}$, $B = L\widetilde{B}$, and $E = L\widetilde{E}$, where L_R^{-1} is the right-side inverse of L. The new reduced-order system can be written as follows:

$$x_{k+1} = \underbrace{X_{\text{res}}[k]\begin{bmatrix}1-\eta_c[k] & 0\\ \eta_c[k] & 1\end{bmatrix}}_{A_k}x_k + \underbrace{\begin{bmatrix}1\\0\end{bmatrix}}_{B}u_k + \underbrace{\begin{bmatrix}0\\\dfrac{m_{\text{air,in}}}{1-X_{\text{EGR}}}\end{bmatrix}}_{E} \tag{4}$$

where $x_k = \begin{bmatrix}M_{\text{fuel}}[k] & M_{\text{gas}}[k]\end{bmatrix}^T$ is the reduced-order state. Note that the new system matrix A_k does not depend on AFR_s anymore. In a similar way, consider the reduced-order controllability matrix calculated as $\mathcal{C}_k = \begin{bmatrix}B & A_kB\end{bmatrix}$. The spectral decomposition of such matrices, showed in Table II, indicates that the reduced-order system is stable and fully controllable. Intuitively, we observe that the control command u_k immediately affects the in-cylinder fuel mass $M_{\text{fuel}}[k+1]$ which will affect the subsequent in-cylinder gas mass $M_{\text{gas}}[k+2]$ though the system dynamics. Hence, the control reaches both states in less than 2 cycles. Even though the proposed model can be used to design a state feedback controller, in practical applications it is not possible to measure the in-cylinder mass using the stock engine sensors. In this study, a certainty equivalence approach was employed where online estimates

$\widehat{x}_k$ were generated and the control was calculated as if they were the true states. To achieve this task, however, accurate cycle-to-cycle estimates of $X_{\text{res}}[k]$ and $\eta_c[k]$ are required.

A. Online State Estimation

Using the stock engine sensors, $m_{\text{air,in}}$ can be obtained from a mass airflow sensor, while X_{EGR} can be measured using an intake oxygen sensor. On the other hand, the cycle-to-cycle values of $X_{\text{res}}[k]$ and $\eta_c[k]$ can be estimated from in-cylinder pressure data $P_\theta[k]$, where θ is the crank angle [42]. The combustion efficiency was estimated as follows:

$$\widehat{\eta}_c[k] = \frac{\widehat{Q}_{\text{gross}}[k]}{\widehat{M}_{\text{fuel}}[k] Q_{\text{LHV}}} \tag{5}$$

where $Q_{\text{LHV}} = 41.61$ MJ/kg is the lower heating value of the RD5-87 fuel, as measured by the ASTM method D240. The gross heat release was estimated from a single-zone analysis neglecting the effects of blow-by and crevice losses [27]:

$$\widehat{Q}_{\text{gross}}[k] = \int_{\text{IVC}}^{\text{EVO}} \frac{1}{\gamma_\theta - 1} V_\theta \frac{dP_\theta[k]}{d\theta} + \frac{\gamma_\theta}{\gamma_\theta - 1} P_\theta[k] \frac{dV_\theta}{d\theta} + \frac{d\widehat{Q}_{\text{HT}}[k]}{d\theta}\, d\theta \tag{6}$$

where V_θ represents the in-cylinder volume as function of the crank angle θ. Such a method considers the change in sensible internal energy (first term), piston work (second term), and heat transfer from the in-cylinder gas to the walls $Q_{\text{HT}}[k]$. The integration was performed with respect to θ during the combustion stage from IVC to EVO. The polytropic coefficient γ_θ also depends on the crank angle. Similar to the approach taken by Tunestal [43], two different values for the polytropic coefficient before and after combustion were considered. The value of $\gamma_C = 1.41$ was used during compression (before combustion) whereas $\gamma_E = 1.30$ was used during expansion (after combustion). During combustion, a linear interpolation was performed between such values. The convective heat transfer to the cylinder walls was estimated as follows:

$$\frac{d\widehat{Q}_{\text{HT}}[k]}{dt} = \text{HT}_{\text{mult}} S_{\text{wall},\theta} \widehat{h}_{\text{Woschni}}[k] (\widehat{T}_\theta[k] - T_{\text{wall}}). \tag{7}$$

Here, $S_{\text{wall},\theta}$ is the cylinder wall surface area, $T_\theta[k]$ is the in-cylinder temperature, and $T_{\text{wall}} = 500$ K is the cylinder wall temperature which was assumed to be constant and homogeneous. The estimated Woschni's heat transfer correlation coefficient $\widehat{h}_{\text{Woschni}}[k]$ was used while the in-cylinder temperature was estimated from the ideal gas law:

$$\widehat{h}_{\text{Woschni}}[k] = 0.013 b^{-0.2} P_\theta[k]^{0.8} \widehat{T}_\theta[k]^{-0.53} v_{\text{gas},\theta}^{0.8} \tag{8}$$

$$\widehat{T}_\theta[k] = \frac{P_\theta[k] V_\theta}{R(\widehat{M}_{\text{fuel}}[k] + \widehat{M}_{\text{gas}}[k])} \tag{9}$$

where b represents the cylinder bore, $v_{\text{gas},\theta}$ denotes the average cylinder gas velocity, and $R = 287$ J/kgK is the ideal gas constant for dry air. The heat transfer multiplier HT_{mult} was introduced as a calibration variable. For the spark/EGR sweep considered in this study, $0.65 \leq \text{HT}_{\text{mult}} \leq 0.85$ increases as spark advance retards. Such values were obtained by matching the average estimated combustion efficiency $\mathbb{E}[\widehat{\eta}_c]$ with the value obtained from the exhaust gas analyzer.

Although several methods for estimating the residual gas fraction can be found in the literature, Maldonado and Kaul [44] showed that the equation for an isentropic exhaust process contributes to an accurate estimation of the system dynamics. With the additional assumptions of zero valve overlap and ideal gas, the residual gas fraction can be estimated as:

$$\widehat{X}_{\text{res}}[k] = \frac{V_{\text{EVC}}}{V_{\text{EVO}}} \left(\frac{P_{\text{EVC}}[k]}{P_{\text{EVO}}[k]} \right)^{1/\gamma_E}. \tag{10}$$

The subscripts indicate that only the values at exhaust valve opening (EVO) and exhaust valve closing (EVC) are needed for the calculation. During the online estimation, however, $P_{\text{EVC}}[k]$ was replaced by the average exhaust manifold pressure $P_{\text{exh}} \approx 1$ bar. This allowed the ORCAS to start the calculations at EVO and enabled the host computer to send the control command to the ECU in the NI cRIO before EVC.

Finally, the state estimates for the next combustion cycle are generated from the LTV system:

$$\widehat{x}_{k+1} = \widehat{A}_k \widehat{x}_k + B u_k + E. \tag{11}$$

Here, $\widehat{A}_k$ is the estimated system matrix using the estimated values for combustion efficiency and residual gas fraction. All in all, a complete heat release analysis is required to estimate the system states. This procedure involves solving equations (5) to (11) simultaneously at every combustion cycle. Figure 4 illustrates the definition of the combustion cycle and shows the block diagram of the online estimation process. The figure emphasizes that the model-based combustion cycle (grey shaded area) is not synchronized with the ECU cycle. For this reason, the control command u_k needs to be calculated and sent to the NI cRIO before the end of the ECU cycle k. The calculation of u_k, however, depends directly on the cost function of the control problem and the online learning algorithm used.

V. Stochastic Optimal Control Problem

Consider the stochastic optimal control problem of choosing the fuel injection quantity, at any cycle k, such that the following one-step-ahead expected cost function is minimized:

$$J_\rho = \mathbb{E}\left[\left(\frac{u_k}{m_{\text{fuel},0}} - 1 \right)^2 + \rho \left(\frac{Q_{\text{gross}}[k+1]}{Q_{\text{gross},0}} - 1 \right)^2 \right]. \tag{12}$$

Here, $m_{\text{fuel},0}$ and $Q_{\text{gross},0}$ are the nominal values of fuel injected and gross heat release for an operating condition. The first term of the cost function penalizes the deviation from $m_{\text{fuel},0}$, which attempts to maintain as much as possible a stoichiometric charge. The second term penalizes the next-cycle deviation from $Q_{\text{gross},0}$, which is used as a measure of instantaneous CCV. The discounting factor $\rho \geq 0$ quantifies the relative importance of the future combustion CCV with respect to the present amount of fuel injected. Using the linearity of expectation and the definition of variance, (12) simplifies to:

$$J_\rho = \left(\frac{u_k}{m_{\text{fuel},0}} - 1 \right)^2 + \rho \left(\frac{\mathbb{E}\left[Q_{\text{gross}}[k+1] \right]}{Q_{\text{gross},0}} - 1 \right)^2 + \rho \frac{\text{Var}\left[Q_{\text{gross}}[k+1] \right]}{Q_{\text{gross},0}^2}. \tag{13}$$

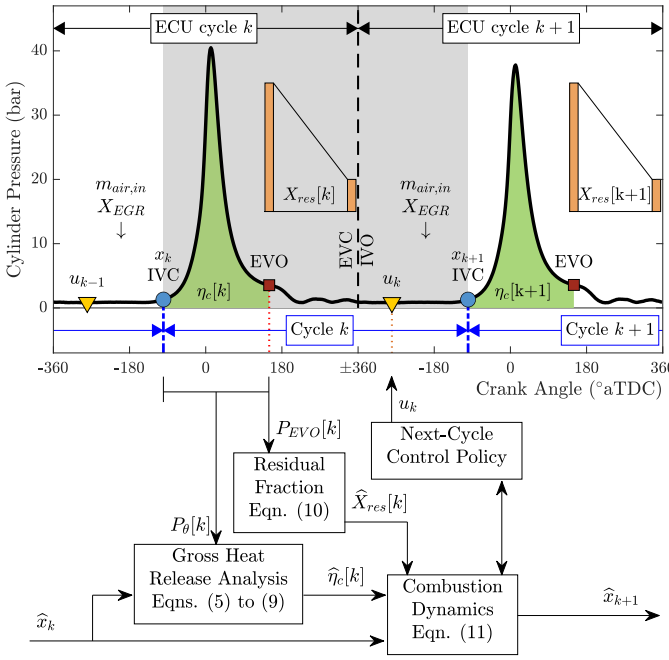

Fig. 4. Combustion cycle definition and state estimation algorithm.

Therefore, finding the optimal next-cycle control command in (13) at cycle k requires the knowledge of the statistical properties of the gross heat release in the next cycle.

A. Model-Based Control Design

According to (5), the statistical properties of the next-cycle gross heat release can be estimated as:

$$\begin{aligned}\mathbb{E}[Q_{\text{gross}}[k{+}1]] &= \mathbb{E}^{\pi}[\eta_c[k{+}1]] \mid \widehat{I}_k, u_k]\widehat{M}_{\text{fuel}}[k{+}1]Q_{\text{LHV}}\\ \text{Var}[Q_{\text{gross}}[k{+}1]] &= \text{Var}^{\pi}[\eta_c[k{+}1] \mid \widehat{I}_k, u_k](\widehat{M}_{\text{fuel}}[k{+}1]Q_{\text{LHV}})^2\end{aligned} \tag{14}$$

where

$$\widehat{I}_k = \{\widehat{x}_k, \widehat{x}_{k-1}, \ldots, \widehat{A}_k, \widehat{A}_{k-1}, \ldots, u_{k-1}, u_{k-2}, \ldots\} \tag{15}$$

represents the information of the system's behavior available at cycle k. The superscript π indicates that the expectation and variance depend on the next-cycle feedback policy $u_k = \pi(\widehat{I}_k)$. Note that, according to the LTV model in (11), $\widehat{M}_{\text{fuel}}[k+1]$ can be calculated given the current state $\widehat{x}_k$, the system matrix $\widehat{A}_k$, and the control command u_k. The next-cycle combustion efficiency, however, is a stochastic variable influenced by combustion CCV. The stochastic component of CCV corresponds to in-cylinder uncertainties such as local turbulence effects, spark energy discharge, and local mixture composition [45]. These perturbations are considered purely random and uncorrelated on a cycle-to-cycle basis. This assumption was proved reasonable by Ameen *et al.* [46] using high-fidelity large-eddy simulations and the parallel perturbation model. In such a study, the CoV of IMEP of consecutive experimental engine cycles under stable combustion was accurately estimated by running simulations in parallel and initializing the turbulence flow field with random uncorrelated perturbations. Therefore, under the assumption that such uncertainties are purely stochastic and independent from each other, x_k can be considered as an information state [47], motivating the following result:

Proposition 1: Let $\{w_k\}_{k\in\mathbb{N}}$ be a sequence of independent and identically distributed (iid) random variables with known probability law representing the stochastic components of CCV, then, for any feedback policy $\pi(\cdot)$:

$$p^{\pi}_{w}(\eta_c[k+1] \mid I_k, u_k) = p_{w_{k+1}}(\eta_c[k+1] \mid x_k, A_k, u_k). \tag{16}$$

Here, $p^{\pi}_{w}(\cdot \mid I_k, u_k)$ is the probability density function (PDF) with respect to the random sequence $\{w_k\}_{k\in\mathbb{N}}$ under the feedback policy $\pi(\cdot)$ given the information up to cycle k.

Proof: Previous studies showed that the combustion efficiency can be written as a function of the in-cylinder composition and the stochastic CCV represented by w:

$$\eta_c[k+1] = g(x_{k+1}, w_{k+1}) \tag{17}$$

where the function $g(\cdot)$ has been approximated using parametric [7], [42] and nonparametric [48], [49] approaches. The LTV model in (11) indicates that x_{k+1} is a function of the stochastic CCV variables $\{w_k, w_{k-1}, \ldots\}$ which are independent of w_{k+1} by assumption. Therefore:

$$\begin{aligned}&p^{\pi}_{w}(\eta_c[k+1] \mid I_k, u_k)\\ &\quad= p^{\pi}_{w_{k+1}}(\eta_c[k+1] \mid x_{k+1} = A_k x_k + B u_k + E)\\ &\quad= p^{\pi}_{w_{k+1}}(\eta_c[k+1] \mid x_k, A_k, u_k)\end{aligned} \tag{18}$$

The first equality indicates that the conditional distribution only depends on the current state, and the PDF is calculated only with respect to w_{k+1}. The second equality is possible since matrices B and E are known. Finally, dependence on the feedback policy $\pi(\cdot)$ can be dropped observing that:

$$p^{\pi}_{w_k}(\eta_c[k] = \eta \mid x_k) = p_{w_k}(w_k \mid g(x_k, w_k) = \eta), \ \forall k \tag{19}$$

which is independent of $\pi(\cdot)$ because the PDF of w_k is known. ■

Another way to interpret Proposition 1 is that $\eta_c[k+1]$ only depends on x_{k+1} and w_{k+1}, according to the model described by (17). Hence, the combustion efficiency only depends on the current state and is independent of previous information I_k. Recall that, in the physical system, x_{k+1} is the in-cylinder state (mass of fuel and gas) and w_{k+1} represents the random perturbation caused by turbulent effects, energy discharge, and local equivalence ratios. Because the state x_{k+1} already contains the information of the fuel injection quantity u_k, the combustion efficiency $\eta_c[k+1]$ does not depend on u_k any more and is entirely determined by x_{k+1} and w_{k+1}. In reality, however, the state x_k was not observable and its estimate was calculated using (11). Nonetheless, the experimental results showed that the certainty equivalence principle adopted in this study can still be advantageous for extending the dilute limit.

Knowledge of the conditional PDF allows the calculation of the conditional mean and variance:

Corollary 1: The conditional expectation and variance of the next-cycle predicted combustion efficiency can be calculated

using only the information at the current cycle (x_k, A_k, and u_k) and are independent of the feedback policy $\pi(\cdot)$. That is:

$$\begin{aligned}\mathbb{E}^{\pi}[\eta_c[k+1] \mid I_k, u_k] &= \mathbb{E}[\eta_c[k+1] \mid x_k, A_k, u_k] \\ \text{Var}^{\pi}[\eta_c[k+1] \mid I_k, u_k] &= \text{Var}[\eta_c[k+1] \mid x_k, A_k, u_k]. \end{aligned} \quad (20)$$

For online implementation, however, the estimates $\widehat{x}_k$ and $\widehat{A}_k$ were used for calculations.

Combining the proposed cost function in (13) with the LTV model in (11) and the results of Corollary 1, the optimal next-cycle feedback policy can be calculated as follows:

$$u_k^* = \pi^*(\widehat{x}_k, \widehat{A}_k) = \underset{u_k \in [u_{\min}[k], u_{\max}]}{\text{argmin}} J_\rho(\widehat{x}_k, \widehat{A}_k, u_k). \quad (21)$$

During the experimental implementation, the control space $[u_{\min}[k], u_{\max}]$ was discretized into 20 equidistant points and the minimizer was chosen based on the corresponding discretized version of $J_\rho(\cdot)$. The maximum allowable amount of fuel injected is a calibration parameter. For this study, the parameter was chosen as $u_{\max} = 1.04 \times m_{\text{fuel},0}$. The lower bound, however, depends on the dilute limit. A reduction of in-cylinder fuel produces a lean gas-fuel mixture with reduced combustion efficiency. Consider using the gas-fuel equivalence ratio as an indicator of the dilute limit with EGR [50]:

$$\lambda_k' = \left(\frac{\widehat{M}_{\text{gas}}[k]}{\widehat{M}_{\text{fuel}}[k]}\right) \frac{1}{\text{AFR}_{\text{s}}}. \quad (22)$$

Let $\lambda'_{\max}$ be the maximum allowable gas-fuel equivalence ratio corresponding to the dilute limit. Such a limit depends on the levels of EGR but is independent of spark advance. Therefore, at any cycle k, the control command should be chosen such that $\lambda'_{k+1} \leq \lambda'_{\max}$. Using the LTV model in (11) the lower bound for the fuel command at cycle k can be calculated as:

$$\begin{aligned} u_{\min}[k] &= u_{\min}(\widehat{x}_k, \widehat{A}_k) \\ &= \frac{\widehat{M}_{\text{gas}}[k+1]}{\lambda'_{\max}\text{AFR}_{\text{s}}} - \underbrace{\widehat{X}_{\text{res}}[k](1-\widehat{\eta}_c[k])\widehat{M}_{\text{fuel}}[k]}_{\widehat{M}_{\text{fuel,res}}[k]}. \end{aligned} \quad (23)$$

The first term calculates the in-cylinder fuel amount required to achieve $\lambda'_{\max}$. The second term corresponds to the residual unburned fuel already contained in the cylinder.

Recall that the optimal feedback policy $\pi^*(\widehat{x}_k, \widehat{A}_k)$ penalizes fuel commands that differ from the stoichiometric value $m_{\text{fuel},0}$. However, combustion cycles with significantly low energy release leave a substantial amount of residual fuel remaining to be used during the next cycle. This implies that an aggressive reduction in the fuel control command is required to avoid high-energy events after misfires and severe partial burns. The maximum amount residual fuel that can be compensated by $u_k = u_{\min}(\widehat{x}_k, \widehat{A}_k)$ can be approximated by:

$$M_{\text{fuel,res}}^{\max}[k] \approx \frac{Q_{\text{gross},0}}{\eta_0 Q_{\text{LHV}}} - u_{\min}(\widehat{x}_k, \widehat{A}_k). \quad (24)$$

Here, η_0 is the nominal combustion efficiency. This approximation was based on (11) and under the assumption that EGR contains no leftover fuel from previous cycles. In this case, if a low-energy event causes the residual fuel to go above $M_{\text{fuel,res}}^{\max}[k]$, then the controller requires a command lower than $u_{\min}(\widehat{x}_k, \widehat{A}_k)$ to achieve $Q_{\text{gross},0}$ in the following cycle. Therefore, to fully utilize the deterministic characteristics of combustion CCV without violating the dilute limit defined by $\lambda'_{\max}$, consider the following augmented feedback policy:

$$m_{\text{fuel,in}}[k] = \begin{cases} \pi^*(\widehat{x}_k, \widehat{A}_k) & \text{if } \widehat{M}_{\text{fuel,res}}[k] < M_{\text{fuel,res}}^{\max}[k] \\ u_{\min}(\widehat{x}_k, \widehat{A}_k) & \text{otherwise.} \end{cases} \quad (25)$$

Another way to interpret (25) is to consider $\pi^*(\widehat{x}_k, \widehat{A}_k)$ as the predictive policy and $u_{\min}(\widehat{x}_k, \widehat{A}_k)$ as the reactive command for low-energy events. During nominal combustion ($\widehat{M}_{\text{fuel,res}}[k] < M_{\text{fuel,res}}^{\max}[k]$), the predictive policy will try to adjust the fuel injection quantity to avoid future low-energy events. However, if a misfire or severe partial burn occurs ($\widehat{M}_{\text{fuel,res}}[k] \geq M_{\text{fuel,res}}^{\max}[k]$), then the fuel command is reduced as much possible without violating the user-defined limit $\lambda'_{\max}$. The implementation of the augmented feedback policy, however, requires the online estimation of the statistical properties of the combustion efficiency.

VI. Online Statistical Learning

The conditional PDF $p(y_k \mid z_k)$ can be estimated from N observations (Y_i, Z_i) for $1 \leq i \leq N$ using the kernel density estimator (KDE) which provides a nonparametric unsupervised estimator for the conditional density as follows [51]:

$$\widehat{p}(y_k \mid z_k) = \frac{\displaystyle\sum_{i=1}^{N} K\left(\frac{Y_i - y_k}{h_y}\right) \prod_{j=1}^{\dim(z)} K\left(\frac{Z_{i,j} - z_{k,j}}{h_{z,j}}\right)}{\displaystyle h_y \sum_{i=1}^{N} \prod_{j=1}^{\dim(z)} K\left(\frac{Z_{i,j} - z_{k,j}}{h_{z,j}}\right)}. \quad (26)$$

Here, $K(r) = (2\pi)^{-0.5}\exp(-0.5r^2)$ is the Gaussian kernel, and h_y, $h_z = \begin{bmatrix} h_{z,1} & \dots & h_{z,\dim(z)} \end{bmatrix}^T$ are the bandwidths. Calibration of the bandwidths was performed offline using the maximum-likelihood leave-one-out cross-validation [52]. The `statsmodels` Python module was employed to find the bandwidths using steady-state data [53]. Such values were kept constant during open-loop and closed-loop operations.

Proposition 2: Using the KDE defined in (26), the first and second estimated conditional moments can be calculated as:

$$\begin{aligned} \widehat{\mathbb{E}}[y_k \mid z_k] &= \sum_{i=1}^{N} \Pi K\left(\frac{Z_i - z_k}{h_z}\right) Y_i \Big/ \sum_{i=1}^{N} \Pi K\left(\frac{Z_i - z_k}{h_z}\right) \\ \widehat{\mathbb{E}}[y_k^2 \mid z_k] &= \sum_{i=1}^{N} \Pi K\left(\frac{Z_i - z_k}{h_z}\right) Y_i^2 \Big/ \sum_{i=1}^{N} \Pi K\left(\frac{Z_i - z_k}{h_z}\right) \\ &\quad + h_y^2. \end{aligned} \quad (27)$$

where

$$\Pi K\left(\frac{Z_i - z_k}{h_z}\right) = \prod_{j=1}^{\dim(z)} K\left(\frac{Z_{i,j} - z_{k,j}}{h_{z,j}}\right). \quad (28)$$

Proof: See Appendix for details. ∎

For this particular study, the response variable is $y_k = \eta_c[k] = \eta_k$ with observations $Y_i = \eta_c[i]$, and the predictor variable is

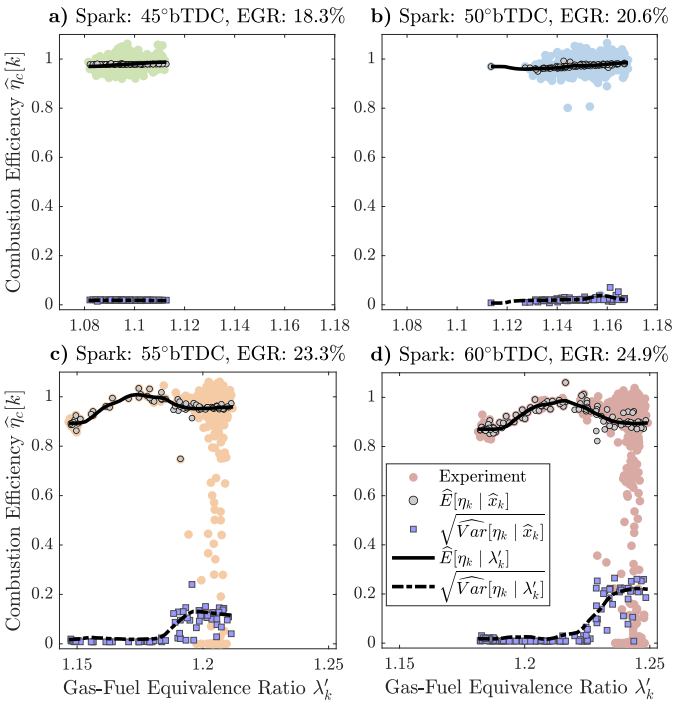

Fig. 5. Estimated conditional mean and variance of $\eta_c[k]$ given the estimated states $\widehat{x}_k$ (opaque markers) or the gas-fuel equivalence ratio λ'_k (lines). The transparent markers show the open-loop data used for estimation.

the state x_k with dimension $\dim(x) = 2$ and observations $Z_i = \begin{bmatrix} Z_{i,1} & Z_{i,2} \end{bmatrix}^T = \begin{bmatrix} \widehat{M}_{\text{fuel}}[i] & \widehat{M}_{\text{gas}}[i] \end{bmatrix}^T$. Finally, using the definition of conditional variance, the estimates of the statistical properties of $\eta_c[k+1]$ can be written as functions of $\widehat{x}_{k+1} = \widehat{A}_k \widehat{x}_k + Bu_k + E$ as follows:

$$\begin{aligned} \mathbb{E}[\eta_c[k+1] \mid \widehat{x}_k, \widehat{A}_k, u_k] &= \widehat{\mathbb{E}}[\eta_{k+1} \mid \widehat{A}_k \widehat{x}_k + Bu_k + E] \\ \text{Var}[\eta_c[k+1] \mid \widehat{x}_k, \widehat{A}_k, u_k] &= \widehat{\mathbb{E}}[\eta_{k+1}^2 \mid \widehat{A}_k \widehat{x}_k + Bu_k + E] \\ &\quad - \Big(\mathbb{E}[\eta_c[k+1] \mid \widehat{x}_k, \widehat{A}_k, u_k]\Big)^2 \end{aligned} \quad (29)$$

Note that the estimator is a scalar map from a two-dimensional space, i.e. $\widehat{\mathbb{E}}[\eta_{k+1} \mid \widehat{x}_{k+1}] \colon \mathbb{R}^2 \mapsto \mathbb{R}$. However, for online implementation, limitations on computational resources might require an estimator of lower order. In such a case, the gas-fuel equivalence ratio, defined in (22), can be considered as a proxy variable for the state. Therefore, the simplified estimator corresponds to the map $\widehat{\mathbb{E}}[\eta_{k+1} \mid \lambda'_{k+1}] \colon \mathbb{R} \mapsto \mathbb{R}$. This approach requires the same calculations as in (27) but simplifies (28) by reducing it to a single component.

Figure 5 shows the comparison between both estimation methods at the same conditions discussed in Fig. 3. For all plots, the transparent markers correspond to the open-loop experimental data used to generate the KDEs, the solid markers represent the KDE using the entire state space, and the black lines represent the KDE using only the gas-fuel equivalence ratio. Note that, as EGR levels increase, the nominal value of the gas-fuel equivalence ratio λ'_0 increases. Table III shows the resulting conditional statistics for both approaches evaluated at λ'_0 and the corresponding nominal state x_0. Similar values in mean and variance were captured

TABLE III
COMPARISON BETWEEN KDEs FOR CONDITIONAL MEAN AND VARIANCE OF COMBUSTION EFFICIENCY AT NOMINAL CONDITIONS

EGR	λ'_0	$\widehat{\mathbb{E}}[\eta_k \mid \lambda'_0]$	$\widehat{\mathbb{E}}[\eta_k \mid x_0]$	$\sqrt{\widehat{\text{Var}}[\eta_k \mid \lambda'_0]}$	$\sqrt{\widehat{\text{Var}}[\eta_k \mid x_0]}$
18.3%	1.10	0.98	0.98	0.019	0.019
20.6%	1.15	0.97	0.98	0.023	0.021
23.3%	1.21	0.96	0.96	0.122	0.123
24.9%	1.24	0.89	0.89	0.221	0.230

by both estimators, showing a decrease in average efficiency and increase in variability as EGR levels increase. For the two conditions with the highest EGR fraction, the cycle-to-cycle values of λ'_k decrease in the cycle after low-energy events occur. After misfires (lowest values of λ'_k) the combustion efficiency decreases to its lowest values. However, after some partial burns, the combustion efficiency increases closer to 98%. This concave shape observed in the $\widehat{\mathbb{E}}[\eta_k \mid \cdot]$ vs λ'_k graph, at high EGR levels, mimics the behavior of the laminar flame speed with respect to equivalence ratio reported in the literature [27]. Although $\widehat{\mathbb{E}}[\eta_k \mid \widehat{x}_k]$ presents a more scattered behavior compared to the reduced order estimator $\widehat{\mathbb{E}}[\eta_k \mid \lambda'_k]$, they both vary within a narrow range. Nonetheless, the estimated variance shows a wider discrepancy around λ'_0. Note that $\widehat{\text{Var}}[\eta_k \mid \lambda'_k]$ looks almost like a non-decreasing function of λ'_k. Using the estimator over the state space, however, we observe that for a small positive number $\varepsilon > 0$ the estimated variance on an ε-neighborhood around the nominal value λ'_0, i.e. $\widehat{\text{Var}}[\eta_k \mid \widehat{x}_k, \lambda'_k \in [\lambda'_0 - \varepsilon, \lambda'_0 + \varepsilon]]$, can be found almost anywhere in the interval $[0, 0.25^2]$. The disparity between the KDEs highlights the information lost when condensing the state space into a one-dimensional value.

Recall that one of the main results of Proposition 1 indicated that the conditional PDF $p(\eta_k \mid x_k)$ is independent of the feedback law. This implies two possibilities: 1) the online estimation can be done solely during open-loop, or 2) the KDE can start with an initial open-loop sample and update the estimation once the closed-loop operation is switched on. If the strategy is divided into a learning phase followed by a control phase starting at cycle L, then the KDE will use a fixed-window buffer to store the open-loop data points (Y_{K-i}, Z_{K-i}) for $0 \leq i \leq N-1$ and $K < L$. On the other hand, if learning and control are performed simultaneously, then the KDE will use a moving-window buffer to store the closed-loop data points (Y_{k-i}, Z_{k-i}) for $0 \leq i \leq N-1$ and $k \in \mathbb{N}$. Therefore, four different learning strategies can be paired with the control algorithm to calculate the optimal policy $\pi^*(\cdot)$. Experiments were conducted using KDEs with learning based on the full state-space $\widehat{p}(\eta_k \mid \widehat{x}_k)$, or the simplified gas-fuel equivalence ratio $\widehat{p}(\eta_k \mid \lambda'_k)$; both KDE strategies were tested using either a fixed-window memory buffer or a moving-window memory buffer. During experimental implementation, a buffer size of $N = 3000$ was used for the fixed and moving-window buffers alike. By using either a fixed or a moving-window buffer, there was not a measurable time difference in computational performance of the rapid-prototyping controller. All the calculations regarding

the optimal control policy were still done in 2 ms.

VII. Experimental Results

The cost function $J_\rho(\widehat{x}_k, \widehat{A}_k, u_k)$ has two conflicting objectives: reducing CCV using fuel injection while maintaining stoichiometric combustion as much as possible. The discounting factor ρ is in charge of the tradeoff between these two goals. Note that if $\rho = 0$ then $\pi^*(\widehat{x}_k, \widehat{A}_k) = m_{\text{fuel},0}$ according to (13), which is the open-loop control command. Therefore, stoichiometric combustion is prioritized when ρ is small. Conversely, as ρ increases the average fuel command will increase in order to reduce combustion CCV by enriching the charge. The sensitivity of the different KDE strategies with respect to ρ, however, is not the same.

A. Sensitivity with Respect to the Discounting Factor

Figure 6 shows the closed-loop experimental results using the optimal feedback policy for different values of the discounting factor ρ at 55°bTDC spark advance and 23.7% EGR fraction. Each data point corresponds to an average value over 2000 cycles. The results on the left column used the full-state conditional PDF $\widehat{p}(\eta_k \mid \widehat{x}_k)$ for estimating the statistical properties of the combustion efficiency, whereas the right column used the lower-dimensional PDF $\widehat{p}(\eta_k \mid \lambda'_k)$ for estimation. The top row corresponds to the additional fuel utilized by the control policy, measured as a percentage with respect to the stoichiometric value. Firstly, note that the domain from where ρ was chosen differs by an order of magnitude between the two KDE strategies, indicating different sensitivities with respect to ρ. When the state was used to predict the statistical properties of the next-cycle combustion efficiency, the feedback policy rapidly increased fuel when $\rho < 0.3$. As $\rho \to 0.95$, the additional fuel increased slower at an almost linear rate. On the other hand, when the gas-fuel equivalence ratio was used for generating estimates, the control policy increased the fuel command linearly as $\rho \to 0.1$. Similar behavior is observed in the reduction of CoV for IMEP (middle row) and gross heat release (bottom row).

The learning phase was conducted using either a fixed-window buffer stored during open-loop (blue solid line) or a moving-window buffer which updates the KDE during closed-loop (green dash-dotted line). The similarity between both buffer types is due to the theoretical outcome of Proposition 1, which stated that learning during open- or closed-loop, within the same region of the state space, yields similar estimates. The differences observed, however, can be attributed to the level of exploration of the state space by the KDE. During open-loop, the KDE generated estimates for a constant fuel command, whereas during closed-loop the KDE observed a wider range of control values, but it also observed a lower number of misfires and partial burns due to the fuel enrichment.

In order to quantify how much the full-state KDE outperforms its simplified version, consider calculating the additional fuel needed to reduce the CoV of IMEP by a fixed percentage. The black dashed and dash-dotted lines pictured in the CoV plots of Fig. 6 show a reduction of 30% and 60% with respect to the open-loop (OL) values, respectively. When $\widehat{p}(\eta_k \mid \widehat{x}_k)$

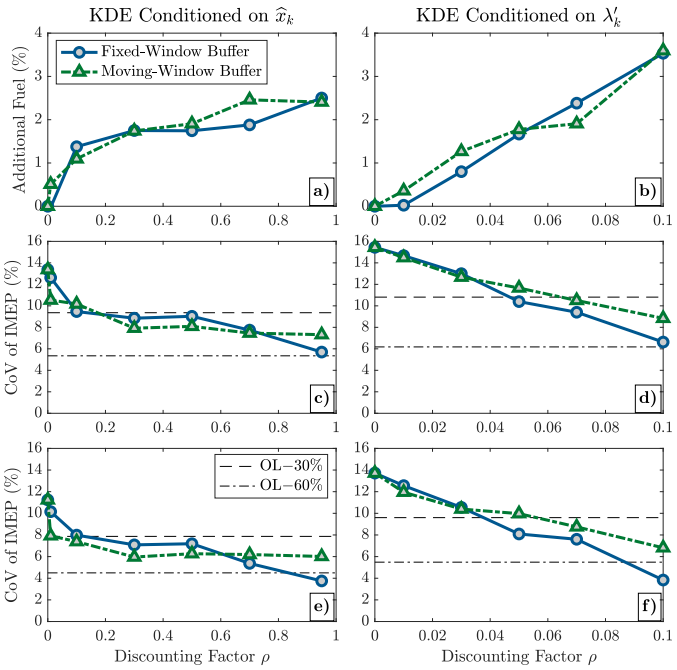

Fig. 6. Experimental closed-loop response for different ρ values using the full state (left) and simplified (right) conditional KDEs using either a fixed-window (solid lines) or moving-window (dash-dotted lines) buffers. Operating condition: 55°bTDC spark advance and 23.7% EGR fraction.

was used for estimation, the controller was able to reduce the CoV of IMEP by 30% by increasing the fuel injection quantity by 1.2% ($\rho = 0.1$). On the other hand, when the simplified $\widehat{p}(\eta_k \mid \lambda'_k)$ was used, the controller generated the same CoV of IMEP reduction by increasing the fuel command by 1.7% ($\rho = 0.05$). Such a difference between the KDE approaches is more notorious when ρ reaches its highest value for both cases. The full-state KDE reduces the CoV of IMEP by nearly 60% using 2.5% additional fuel, whereas the lower-dimensional KDE requires 3.5% additional fuel to achieve the same goal. Therefore, the effectiveness of the simplified KDE approach using λ'_k is inversely proportional to the value of ρ.

A closer look at the cycle-to-cycle behavior of the optimal control policy is provided in Fig. 7. The time series of the fuel command (top) and gross heat release (bottom) for 200 cycles are depicted during open-loop ($\rho = 0$) and closed-loop using the full-state KDE with a fixed-window buffer. The black dashed and dash-dotted lines indicate a 1% and 2% increase with respect to the open-loop fuel command, respectively. When $\rho = 0.01$, the controller stayed close to the open-loop value and occasionally jumped to inject 1% additional fuel when the uncertainty of the next-cycle event was high. Recall that the uncertainty, quantified by the conditional variance $\widehat{\text{Var}}[\eta_k \mid \widehat{x}_k]$, increases in regions of the state space where misfires and partial burns occur. This switching behavior was identified in a previous simulation study by the authors [29]. The prediction of misfires and partial burns, however, was not always accurate and such low-energy events occurred during closed-loop operation. Recall that the augmented control policy described in (25) drastically reduces the fuel command after a low-energy event occurs.

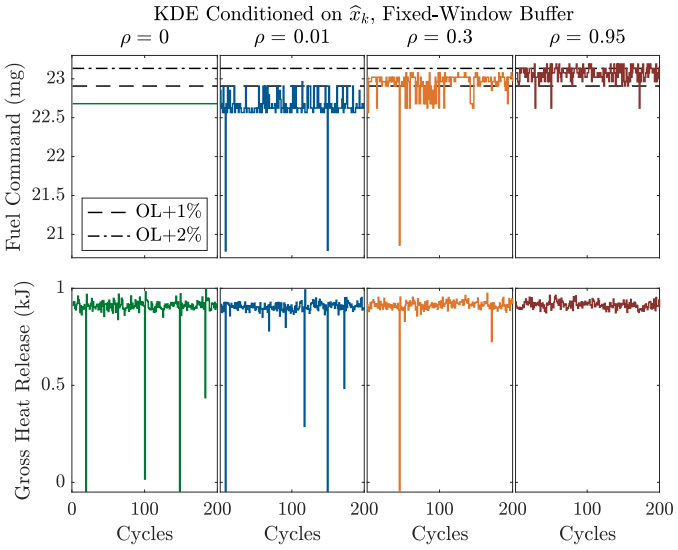

Fig. 7. Time series of fuel command (top) and Q_{gross} (bottom) for different ρ values at 55°bTDC spark and 23.7% EGR, segments correspond to 200 cycles.

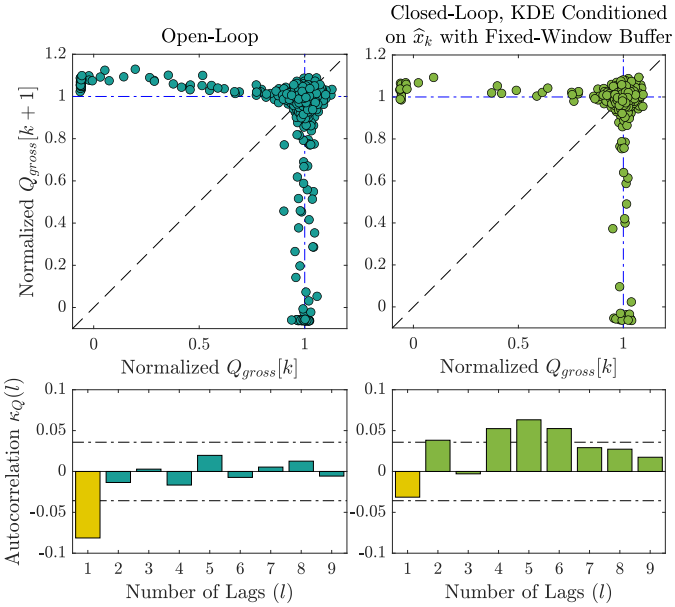

Fig. 8. Comparison between the return map (top) and the autocorrelation coefficient (bottom) of Q_{gross} during open-loop (left) and closed-loop (right).

Such a behavior can be seen when $m_{\text{fuel,in}}[k] < 21$ mg. When $\rho = 0.3$, the controller hovered around an average value 1.5% higher than the open-loop command. In this case, the controller jumped back to the stoichiometric value when it estimated that the probability of a misfire event was low. Finally, at $\rho = 0.95$ the controller stayed around a 2% fuel increase with a minimum incursion into values closer to stoichiometric. This trend was expected as a richer mixture provides a more stable combustion at the cost of additional fuel consumption. Calibration of ρ is important for balancing such a tradeoff. The sensitivity analysis highlights the importance of choosing an appropriate value of the discounting factor ρ depending on the conditional KDE method, the learning strategy, and the overall goal of the closed-loop system. Moreover, the calibrated value of ρ depends on the EGR fraction, which alters the region of the state space, and the spark advance, which changes the CCV dominant effects between misfires and partial burns.

B. Effectiveness of Using Next-Cycle Deterministic Dynamics

The discounting factor ρ also determines the level of actuation done by the controller. Recall that if $\rho \to 0$ then the fuel injection command approaches a constant value of $m_{\text{fuel,0}}$ and does not fully utilize the next-cycle deterministic characteristics of CCV. In order to determine if the controller exploits the next-cycle correlations found in the data, consider examining the return map and the serial autocorrelation coefficient of Q_{gross}. The top row of Fig. 8 shows the return maps of the open-loop (left) and closed-loop (right) values of Q_{gross} recorded at 55°bTDC spark advance and 23.7% EGR fraction. For the closed-loop system, the feedback policy was calculated using the full-state KDE with a fixed-window buffer and $\rho = 0.2$ was calibrated to generate a 1.2% fuel increase. As previously discussed, the open-loop return map presents an asymmetric shape with respect to the $x = y$ diagonal, implying next-cycle correlation. The blue dash-dotted horizontal and vertical lines help to distinguish the asymmetric shape of the open-loop plot. Note that the upper portion is located above the horizontal line while the lower portion, on the contrary, aligns very well with the vertical line. In the case of the closed-loop return map, the upper portion of the plots aligns in closer proximity with the horizontal line, indicating a better symmetry and less next-cycle correlation.

The level of next-cycle correlation can be quantified by the serial autocorrelation coefficient, defined as:

$$\kappa_Q(l) = \frac{\mathbb{E}\left[(Q_{\text{gross}}[k] - \mu_Q)(Q_{\text{gross}}[k-l] - \mu_Q)\right]}{\text{Var}[Q_{\text{gross}}]} \tag{30}$$

where l is the lag and $\mu_Q = \mathbb{E}[Q_{\text{gross}}]$ is the population mean. The bar plots in the bottom row of Fig. 8 show the autocorrelation $\kappa_Q(l)$ for lags between $1 \leq l \leq 9$. The dash-dotted lines indicate the 95% confidence interval for the autocorrelation, indicating the values within that interval are not statistically significant ($\kappa_Q(l) = 0$). Previous studies have shown that cycle-to-cycle features during stable combustion (before the dilute limit) are statistically uncorrelated, rendering $\kappa_Q(l) = 0 \ \forall l > 0$ [54]. At the dilute limit, however, the left plot shows that the autocorrelation coefficient of the open-loop time series exhibits a statistically significant value for next-cycle correlation ($l = 1$). On the other hand, the $l = 1$ autocorrelation during closed-loop, highlighted in the right bar plot, is statistically equal to zero. This implies that the controller was effectively decoupling combustion cycles, highlighting the advantage of feedback control versus constant fuel enrichment which cannot take advantage of next-cycle deterministic effects. In addition, this observation brings up another tradeoff in the control problem where lower values of ρ are desired for stoichiometric combustion but ρ needs to be large enough to exploit deterministic effects. With this caveat in mind, closed-loop experiments were conducted for all operating conditions considered in this study with ρ preferentially calibrated for low fuel enrichment.

C. Effectiveness of CoV Reduction Past the EGR Dilute Limit

The results of 3000 experimental combustion cycles under closed-loop operation across different spark and EGR levels using the full-state KDE with a fixed-window buffer are summarized in Fig. 9. The top and middle contour plots show the closed-loop CoV values of IMEP and gross heat release, respectively. Similar to Fig. 2, the markers help to delimit the different combustion regions. The dashed-dotted, dashed, and dotted lines represent the combustion phasing moving from retarded to advanced conditions, which did not change significantly with respect to the open-loop case. The bottom contour plot shows the additional fuel used by the feedback policy, as a percentage increased over the stoichiometric value. The values in the text boxes correspond to the discounting factor ρ used in each condition. It was observed that, in general, ρ is smaller in the misfire region compared to the values in the partial burn region, which indicates that misfires will force the controller to use more fuel compared to other low-energy events. Compared with the open-loop case, the CoV values were reduced across all conditions on average by around 20% using at most 1.2% extra fuel at retarded conditions and 1.4% extra fuel at advanced conditions. In particular, at optimal combustion phasing, the dilute limit was extended from 18.5% to almost 21% EGR fraction by using approximately 0.5% additional fuel. Since the control policy depends on the learning strategy used by the KDE, however, the example in Fig. 9 corresponds to only one out of the four possible feedback policies.

In order to determine which learning approach (out of four possible) best suits the optimal control policy, consider using the average indicated fuel conversion efficiency:

$$\eta_i = \frac{\mathbb{E}[\text{IMEP}]V_d}{\mathbb{E}[m_{\text{fuel,in}}]Q_{\text{LHV}}} \tag{31}$$

where V_d is the displacement volume. Therefore, the average increase in indicated fuel conversion efficiency due to closed-loop control, relative to open-loop, can be calculated as:

$$\Delta\eta_i = \frac{\eta_i^{\text{CL}}}{\eta_i^{\text{OL}}} - 1 = (\Delta\text{IMEP} + 1)\,(\Delta m_{\text{fuel,in}} + 1)^{-1} - 1 \tag{32}$$

where $\Delta\text{IMEP} = \mathbb{E}[\text{IMEP}^{\text{CL}}]/\mathbb{E}[\text{IMEP}^{\text{OL}}] - 1$ and $\Delta m_{\text{fuel,in}} = \mathbb{E}[m_{\text{fuel,in}}^{\text{CL}}]/m_{\text{fuel,0}} - 1$ are the average increases in IMEP and fuel injection quantity with respect to open-loop, respectively. Figure 10 shows the relative increase $\Delta\eta_i$ for all four possible learning strategies during a spark/EGR sweep in closed-loop. The top row compares the performance of the full-state KDE (subplot a) against the simplified KDE (subplot b). Even though both estimators achieved a maximum value of $\max\Delta\eta_i = 1.9\%$ (boxed text) at the highest levels of EGR, the full-state KDE does so at advanced combustion phasing whereas the simplified KDE achieves the maximum at retarded phasing. More importantly, the level curve $\Delta\eta_i = 0.5\%$, pictured by the black dash-dotted line, indicates that increments in η_i are significant across more operating conditions when using the full-state KDE compared to the simplified approach. The bottom row of Fig. 10 shows the same KDE comparison using a moving-window buffer for learning. The overall behavior of the full-state KDE (left column) is similar

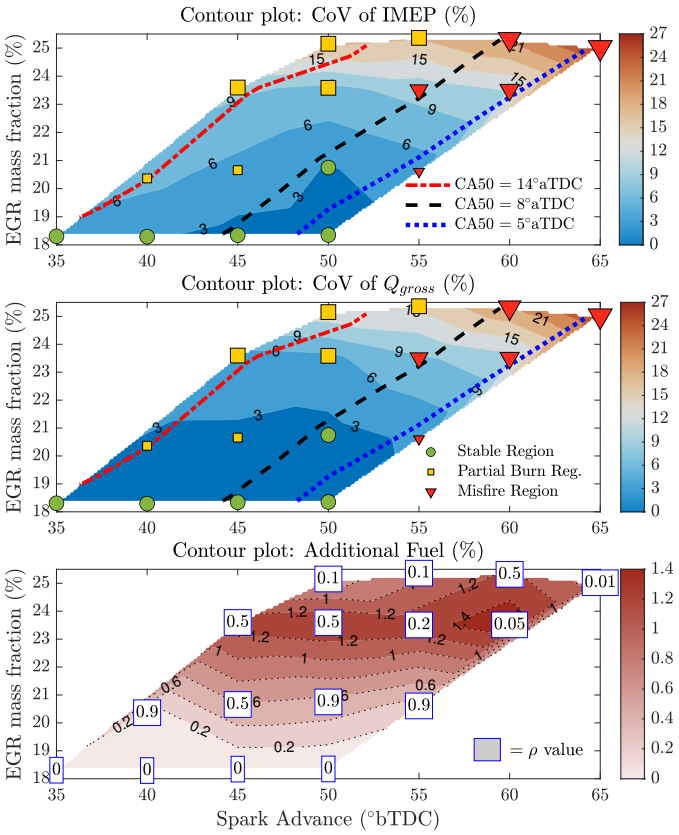

Fig. 9. Experimental closed-loop values for the CoV of IMEP (top), CoV of Q_{gross} (middle), and additional fuel injection quantity used by the control (bottom) during a spark/EGR sweep. The optimal control policy was based on the full-state KDE using a fixed-window buffer stored during open-loop.

using either buffer. However, the case with a moving-window buffer (subplot c) shows a smaller increase in η_i at high EGR levels and advanced sparked compared to the case with a fixed-window buffer. This is a consequence of the learning happening during closed-loop where fewer misfires events are observed, compared to open-loop. On the other hand, the right column shows that the overall effectiveness in increasing η_i using the simplified KDE is similar for both buffer types. The only noticeable difference is the change in location of the maximum increment of η_i, which is located at advanced spark conditions when using the moving-window buffer (subplot d).

The increase in fuel conversion efficiency only takes into account the changes of $\mathbb{E}[\text{IMEP}]$. To determine the effectiveness of the controller in reducing CCV, however, the changes in $\text{Var}[\text{IMEP}]$ should also be included in the analysis. Therefore, similar to (32), consider quantifying the effectiveness of CCV reduction by the feedback policy as follows:

$$\Omega = (\Delta\text{CoV}_{\text{IMEP}})\,(\Delta m_{\text{fuel,in}})^{-1} \tag{33}$$

where $\Delta\text{CoV}_{\text{IMEP}} = 1 - \text{CoV}_{\text{IMEP}}^{\text{CL}}/\text{CoV}_{\text{IMEP}}^{\text{OL}}$ is the reduction of CoV of IMEP due to the feedback policy. The value of Ω quantifies the percentage of CoV reduction per percentage of additional fuel used during closed-loop. An effective feedback policy will decrease CoV as much as possible with the minimum amount of extra fuel. Thus, with both effects combined, the best control strategy will maximize Ω. Figure 11

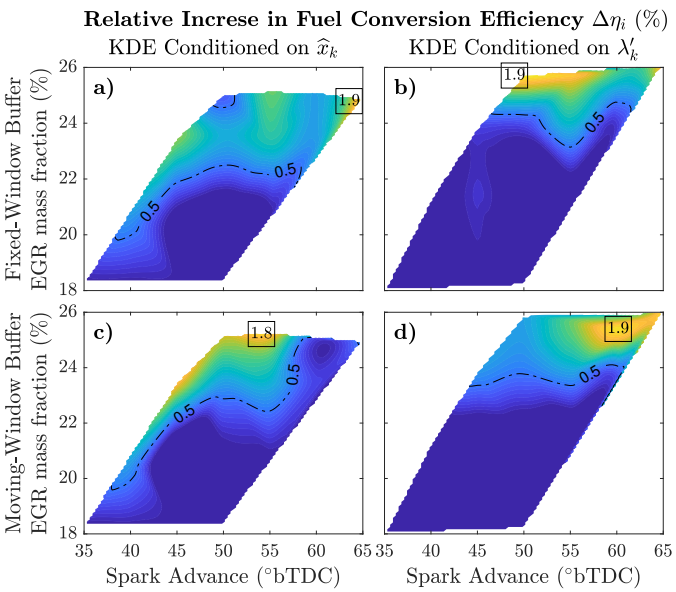

Fig. 10. Relative increase in average η_i during a spark/EGR sweep in closed-loop based on the full-state (left) and simplified (right) KDEs using either a fixed-window buffer (top row) or a moving-window buffer (bottom row). Boxed text indicates the location and magnitude of the maximum value.

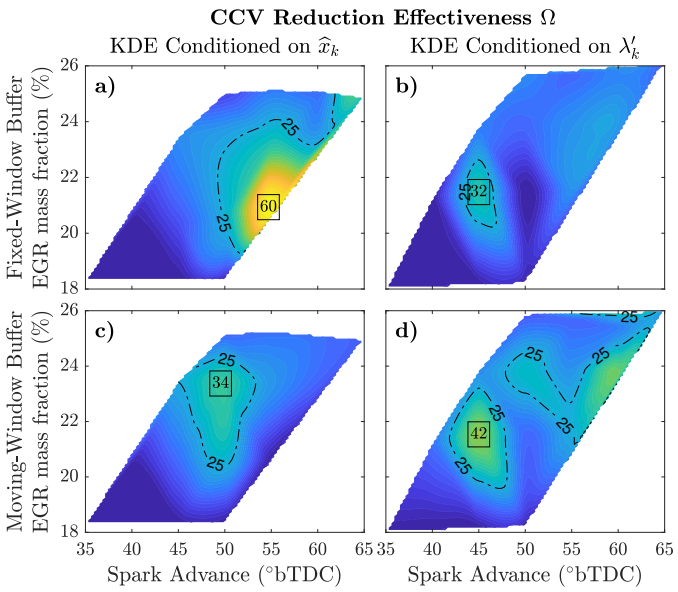

Fig. 11. CCV reduction effectiveness Ω during a spark/EGR sweep in closed-loop control based on the full-state (left) and simplified (right) KDEs using either a fixed-window buffer (top row) or a moving-window buffer (bottom row). Boxed text indicates the location and magnitude of the maximum value.

shows the CCV reduction effectiveness Ω for all four possible learning strategies during a spark/EGR sweep in closed-loop. As expected, the top row indicates that Ω is higher when the conditional PDF $\widehat{p}(\eta_k \mid \widehat{x}_k)$ (left column) was used, suggesting a maximum reduction of 60% CoV by using 1% additional fuel during advanced spark conditions (subplot a). When a moving-window buffer was used (subplot c), however, the overall effectiveness of the full-state KDE decreased and, similar to $\Delta\eta_i$, the maximum value shifted towards retarded spark conditions. On the other hand, the simplified KDE (right column) maintains the maximum value of Ω at retarded spark conditions for both buffer types. However, the overall value of Ω across conditions increased when the moving-window buffer was used (subplot d).

In conclusion, the experimental results showed that if the optimal policy is paired with a full-state KDE using a fixed-window buffer based on open-loop data, then the dilute limit at optimal combustion phasing can be extended from 18.5% to almost 21%. In addition, such a controller achieved the highest values on both effectiveness quantifiers $\Delta\eta_i$ and Ω at advanced spark conditions. If computational power is limited, the simplified KDE presents a good alternative to the problem of CCV reduction. In particular, the simplified KDE with a moving-window buffer maximizes $\Delta\eta_i$ at advanced combustion phasing but presents a higher CCV reduction effectiveness Ω at retarded phasing. However, if CCV reduction is desired at retarded phasing (e.g., during cold starts) a KDE with a moving-window buffer can be more effective.

D. Comparison to Neural-Network-Based Control

Control strategies using neural networks (NN) have been previously applied to the dilute combustion control problem in order to deal with the nonlinearities, modeling issues, and chaotic behavior observed past the dilute limit. Artificial neural networks (ANN) have been used by Vance *et al.* [55] for lean combustion stability control, whereas Singh *et al.* [56] and Vance *et al.* [57], [58] used them for EGR-diluted conditions. More recently, spiking neural networks (SNN) have been used as control agents since they incorporate the notion of time and causality into how they process information, making them better than traditional ANN at control tasks. All the previously mentioned NN-based controllers are similar to the policy proposed in this study in the sense that 1) they require a state estimator to generate the input layer, 2) the output layer corresponds to the fuel injection quantity command, and 3) the optimized NN is chosen based on a CCV minimization criterion. The main difference, however, is that the NN-based methods require offline training and rely on appropriate modeling of the system described by (1). Thus, the choice of modeling determines the performance of the NN controllers.

The best performing KDE-based strategy found in this study (using full-state KDE with a fixed-window buffer) was compared against the best performing SNN-based controller developed in Maldonado *et al.* [59]. The experimental results for both strategies recorded at optimal combustion phasing and similar engine operating conditions are compared in Fig. 12. The top plot shows the resulting CoV of IMEP during closed-loop while the second plot shows the percentage of additional fuel used by the controller. Although both strategies were able to reduce the overall CoV, the KDE-based controller extended the dilute limit closer to 21% EGR fraction with respect to the industry limit of 3% CoV of IMEP. Moreover, the KDE-based strategy achieved this with lower additional fuel. The small relative increase in indicated fuel conversion efficiency suggests a high sensitivity to small perturbations in fuel, which is also captured by the high value of the CCV reduction effectiveness Ω. For all the different EGR levels,

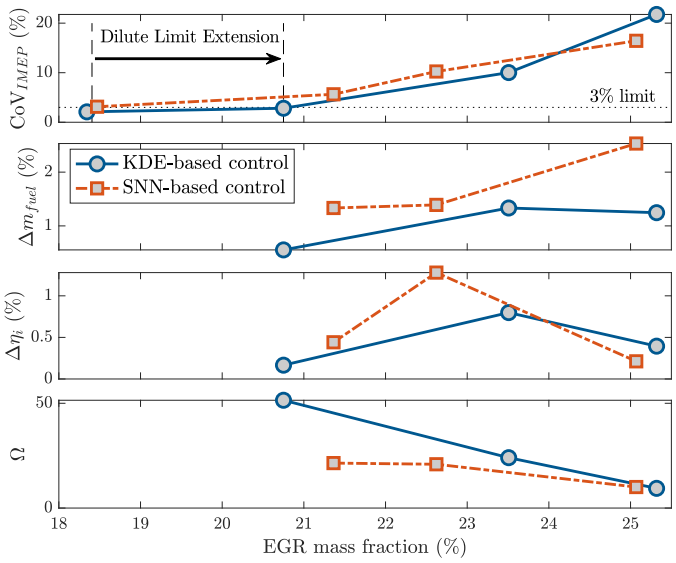

Fig. 12. Comparison of closed-loop CoV of IMEP, additional fuel used, relative indicate fuel conversion efficiency increase, and CCV reduction effectiveness Ω between the SNN-based controller developed in Maldonado *et al.* [59] (dash-dotted line) and the KDE-based controller (solid line).

the SNN-based controller used more additional fuel than the KDE-based controller. However, the values of CoV of IMEP for the SNN-based controller are higher for EGR levels lower than 24%. Even though the higher fuel enrichment of the SNN-based controller generated a larger increase in indicated fuel conversion efficiency, the effectiveness Ω is significantly smaller compared to the KDE-based controller. At 25% EGR fraction, the SNN-based controller generated a lower CoV compared to the KDE-based controller, but it required a significantly higher amount of additional fuel (>2%) which ultimately reduced the performance metrics $\Delta\eta_i$ and Ω. The difference in performance is most likely due to the advantage of online estimation using the KDE compared to the offline training needed for the SNN. All in all, the results showed that the proposed method performs better at extending the dilute limit compared to previous state-of-the-art controllers. In this case, the dilute limit was extended from 18.5% to 21% EGR fraction with maximum CCV reduction effectiveness Ω using 0.5% additional fuel but increasing the average indicated fuel conversion efficiency η_i by 0.2%.

VIII. Conclusion and Outlook

This experimental study evaluated the efficacy of a model-based stochastic optimal combustion control strategy at extending the dilute limit by adjusting the fuel injection quantity. A discrete-time LTV system was used to model the interactions between combustion cycles and generate predictions regarding next-cycle combustion behavior. The controllability properties of the system were analyzed and a fully controllable reduced-order model was proposed. An online estimation algorithm based on in-cylinder pressure data was described for estimating the system states which are not measurable with stock engine sensors. A stochastic optimal control problem was formulated where the cost function consists of three main components: 1) a penalty on changes in the next-cycle heat release, which was used as proxy for combustion CCV, 2) a penalty on changes in fuel injection quantity, which attempts to maintain stoichiometric combustion as much as possible, and 3) a discounting factor, which adjusts the tradeoff between CCV reduction and fuel enrichment. Using a model-based design, the stochastic optimal control problem can be solved if the first and second statistical moments of the cycle-to-cycle combustion efficiency are known. A KDE was used to learn the statistical moments based on previously recorded data. In particular, the KDE was used to estimate the conditional PDF of $\eta_c[k] \in \mathbb{R}$ given the state $x_k \in \mathbb{R}^2$. The theoretical properties of the system, however, indicated that the conditional PDF can be learned during open-loop, using a fixed-window buffer, or during closed-loop, using a moving-window buffer. In addition, a simplified KDE was proposed were $\eta_c[k]$ was estimated using the scalar gas-to-fuel equivalence ratio $\lambda'_k \in \mathbb{R}$.

Experiments were conducted to evaluate the effectiveness of the feedback policy at reducing CCV. The experimental results indicated that care must be taken when calibrating the value of the discounting factor ρ, which dependents on the KDE method (full-state of simplified). In general, as ρ increases the combustion CCV decreases due to fuel enrichment. However, the full-state KDE uses less additional fuel to reduce CCV compared to the simplified KDE. Additionally, the value of ρ is also tied to the ability of the feedback policy at taking advantage of the deterministic properties of the system. During a spark/EGR sweep past the dilute limit, the feedback policy was implemented and the discounting factor ρ was calibrated at each condition in order to generate, on average, a 1% fuel quantity increase. The results showed that, on average, a 20% reduction on CoV of IMEP was possible using the controller. In order to compare the four possible KDE strategies (full-state vs. simplified and fixed-window buffer vs. moving-window buffer), the relative average increase in indicated fuel conversion efficiency $\Delta\eta_i$ due to the corresponding feedback policy was used. This metric indicates how much more efficient the closed-loop system is with respect to the open-loop. Furthermore, the CCV reduction effectiveness Ω was defined to determine which feedback policy can reduce the CoV of IMEP with the minimum amount of additional fuel. The results indicated that the full-state KDE with a fixed-window buffer had the best performance during optimal combustion phasing. In fact, the dilute limit was extended from 18.5% to 21% EGR using 0.5% additional fuel but increasing η_i by 0.2%. If the controller is meant to be used at retarded combustion phasing (e.g., during cold starts), then the simplified KDE with a moving-window buffer can be more effective. Finally, the feedback policy proposed in this study was compared to a previously developed artificial intelligence-based method using spiking neural networks. The results suggest that the KDE-based method is more effective at reducing CCV with a minimum amount of additional fuel compared to the SNN-based method, mainly due to the advantages of online learning.

This study was designed to understand the theoretical properties and practical limitations of a stochastic optimal feedback policy enhanced by online learning of the cycle-to-cycle combustion dynamics. However, in its current form,

the controller will not be compatible with a standard TWC that requires stoichiometric combustion. In future work, it is envisioned that the feedback policy described in this study will be paired with a traditional proportional-integral (PI) controller based on an exhaust oxygen sensor, as previously done in Maldonado *et al.* [59]. By doing this, the PI controller with slow dynamics will maintain on average a stoichiometric charge while the next-cycle controller with fast dynamics will perform small adjustments to reduce CCV and extend the dilute limit. Given the benefits observed from online learning, future work will investigate the feasibility of real-time online training of AI-based methods (such as SNN) which can be efficiently deployed in neuromorphic hardware and do not require large buffers to store data.

APPENDIX
PROOF OF PROPOSITION 2

Let $\{(Y_i, Z_i)\}_{1\leq i\leq N}$ be a series of N observations where the response variable is $Y_i \in \mathbb{R}$ and the predictor variables are $Z_i \in \mathbb{R}^{\dim(z)}$. The m-th moment of the estimated conditional PDF $\widehat{p}(y \mid z)$, can be calculated as:

$$\widehat{\mathbb{E}}[y^m \mid z] = \int_{\mathbb{R}} y^m \widehat{p}(y \mid z) dy$$
$$= \frac{\displaystyle\sum_{i=1}^{N} \prod_{j=1}^{\dim(z)} K\left(\frac{Z_{i,j} - z_j}{h_{z,j}}\right) \overbrace{\int_{\mathbb{R}} \frac{y^m}{h_y} K\left(\frac{Y_i - y}{h_y}\right) dy}^{\mathbb{I}_m(Y_i, h_y)}}{\displaystyle\sum_{i=1}^{N} \prod_{j=1}^{\dim(z)} K\left(\frac{Z_{i,j} - z_j}{h_{z,j}}\right)}.$$

The first equality results from the definition of conditional moment. The second equality results after substituting $\widehat{p}(y \mid z)$ by the KDE in (26). Solving the integral within the expression:

$$\begin{aligned}
\mathbb{I}_m(Y_i, h_y) &= \int_{\mathbb{R}} \frac{y^m}{h_y} K\left(\frac{Y_i - y}{h_y}\right) dy \\
&= \int_{\mathbb{R}} (Y_i - h_y r)^m K(r) dr \\
&= \sum_{p=0}^{m} \binom{m}{p} Y_i^{m-p} (-h_y)^p \int_{\mathbb{R}} r^p K(r) dr \\
&= \sum_{p=0, p \text{ even}}^{m} \binom{m}{p} Y_i^{m-p} h_y^p (p-1)!! \ .
\end{aligned}$$

The second equality is obtained after the change of variable $y = Y_i - h_y r$. The third equality is obtained after applying the binomial theorem, where $\binom{\cdot}{\cdot}$ denotes the binomial coefficient. The final equality results from the values of the moments of a standard Gaussian random variable. Note that the sum only includes the terms when p is even. Here, $(\cdot)!!$ denotes the double factorial and $(-1)!! = 1$. Calculating the value of the integral for $m \in \{1, 2\}$:

$$\mathbb{I}_1(Y_i, h_y) = Y_i \quad \text{and} \quad \mathbb{I}_2(Y_i, h_y) = Y_i^2 + h_y^2.$$

Substituting this in the original expression yields the desired results for $\widehat{\mathbb{E}}[y \mid z]$ and $\widehat{\mathbb{E}}[y^2 \mid z]$. ■

ACKNOWLEDGMENT

This research was supported by the DOE Office of Energy Efficiency and Renewable Energy (EERE), Vehicle Technologies Office (VTO), under the guidance of Gurpreet Singh and Michael Weismiller, and used resources at the National Transportation Research Center, a DOE-EERE User Facility at Oak Ridge National Laboratory.

REFERENCES

[1] U.S. Energy Information Administration, "Annual Energy Outlook 2021," U.S. Department of Energy, Tech. Rep., 2021.

[2] T. Alger, J. Gingrich, C. Roberts, and B. Mangold, "Cooled exhaust-gas recirculation for fuel economy and emissions improvement in gasoline engines," *International Journal of Engine Research*, vol. 12, no. 3, pp. 252–264, 2011.

[3] P. G. Aleiferis, A. M. K. P. Taylor, J. H. Whitelaw, K. Ishii, and Y. Urata, "Cyclic Variations of Initial Flame Kernel Growth in a Honda VTEC-E Lean-Burn Spark-Ignition Engine," in *SAE Technical Paper 2000-01-1207*. SAE International, 03 2000.

[4] H. Lian, J. B. Martz, B. P. Maldonado, A. G. Stefanopoulou, K. Zaseck, J. Wilkie, O. Nitulescu, and M. Ehara, "Prediction of Flame Burning Velocity at Early Flame Development Time With High Exhaust Gas Recirculation and Spark Advance," *Journal of Engineering for Gas Turbines and Power*, vol. 139, no. 8, pp. 082 801–082 801–9, 03 2017.

[5] J. Cha, J. Kwon, Y. Cho, and S. Park, "The effect of exhaust gas recirculation (EGR) on combustion stability, engine performance and exhaust emissions in a gasoline engine," *KSME International Journal*, vol. 15, no. 10, pp. 1442–1450, 2001.

[6] A. A. Quader, "Lean Combustion and the Misfire Limit in Spark Ignition Engines," in *SAE Technical Paper 741055*. SAE International, 1974, pp. 3274–3296.

[7] C. S. Daw, C. E. A. Finney, J. B. Green, M. B. Kennel, J. F. Thomas, and F. T. Connolly, "A Simple Model for Cyclic Variations in a Spark-Ignition Engine," in *SAE Technical Paper 962086*. SAE International, 10 1996.

[8] C. S. Daw, J. B. Green, R. M. Wagner, C. E. A. Finney, L. I. Davis, L. A. Feldkamp, J. W. Hoard, F. Yuan, and F. T. Connolly, "Controlling Cyclic Combustion Variations in Lean-Fueled Spark-Ignition Engines," *AIP Conference Proceedings*, vol. 622, no. 1, pp. 265–277, 2002.

[9] B. P. Maldonado, K. Zaseck, E. Kitagawa, and A. G. Stefanopoulou, "Closed-Loop Control of Combustion Initiation and Combustion Duration," *IEEE Transactions on Control Systems Technology*, vol. 28, no. 3, pp. 936–950, 2020.

[10] B. P. Maldonado, J. S. Freudenberg, and A. G. Stefanopoulou, "Stochastic Feedback Combustion Control at High Dilution Limit," in *2018 Annual American Control Conference (ACC)*, 2018, pp. 1598–1603.

[11] B. Kaul, R. Wagner, and J. Green, "Analysis of Cyclic Variability of Heat Release for High-EGR GDI Engine Operation with Observations on Implications for Effective Control," *SAE Int. J. Engines*, vol. 6, no. 1, pp. 132–141, 04 2013.

[12] C. E. A. Finney, B. C. Kaul, C. S. Daw, R. M. Wagner, K. D. Edwards, and J. B. J. Green, "Invited Review: A Review of Deterministic Effects in Cyclic Variability of Internal Combustion Engines," *International Journal of Engine Research*, vol. 16, no. 3, pp. 366–378, 2015.

[13] B. P. Maldonado and A. G. Stefanopoulou, "Non-Equiprobable Statistical Analysis of Misfires and Partial Burns for Cycle-to-Cycle Control of Combustion Variability," in *Proceedings of the ASME 2018 Internal Combustion Engine Division Fall Technical Conference*. ASME, 2018, p. V002T05A003.

[14] B. Maldonado, A. Stefanopoulou, R. Scarcelli, and S. Som, "Characteristics of Cycle-to-Cycle Combustion Variability at Partial-Burn Limited and Misfire Limited Spark Timing Under Highly Diluted Conditions," in *Proceedings of the ASME 2019 Internal Combustion Engine Division Fall Technical Conference*, 10 2019, p. V001T03A018.

[15] R. Stiffler, B. Kaul, and J. Drallmeier, "Cyclic dynamics of misfires and partial burns in a dilute spark-ignition engine," *Proceedings of the Institution of Mechanical Engineers, Part D: Journal of Automobile Engineering*, vol. 235, no. 2-3, pp. 333–345, 2021.

[16] T. Wallner, J. M. Sevik, R. Scarcelli, B. C. Kaul, and R. M. Wagner, "Effects of Ignition and Injection Perturbation under Lean and Dilute GDI Engine Operation," in *JSAE/SAE 2015 International Powertrains, Fuels & Lubricants Meeting*. SAE International, 2015.

[17] G. G. Zhu, I. Haskara, and J. Winkelman, "Closed-Loop Ignition Timing Control for SI Engines Using Ionization Current Feedback," *IEEE Transactions on Control Systems Technology*, vol. 15, no. 3, pp. 416–427, 2007.

[18] Q. Zhu, S. Wang, R. Prucka, M. Prucka, and H. Dourra, "Model-Based Control-Oriented Combustion Phasing Feedback for Fast CA50 Estimation," *SAE International Journal of Engines*, vol. 8, no. 3, pp. 997–1004, 2015.

[19] P. Emiliano, "Spark Ignition Feedback Control by Means of Combustion Phase Indicators on Steady and Transient Operation," *Journal of Dynamic Systems, Measurement, and Control*, vol. 136, no. 5, pp. 051 021–051 021–10, 2014.

[20] B. Xiao, S. Wang, and R. G. Prucka, "A Semi-Physical Artificial Neural Network for Feed Forward Ignition Timing Control of Multi-Fuel SI Engines," in *SAE Technical Paper 2013-01-0324*.

[21] Y. Zhang and T. Shen, "Cylinder pressure based combustion phase optimization and control in spark-ignited engines," *Control Theory and Technology*, vol. 15, no. 2, pp. 83–91, 2017.

[22] H. Di, Y. Zhang, and T. Shen, "Chaos theory-based time series analysis of in-cylinder pressure and its application in combustion control of SI engines," *Journal of Thermal Science and Technology*, vol. 15, no. 1, pp. JTST0001–JTST0001, 2020.

[23] B. P. Maldonado and A. G. Stefanopoulou, "Cycle-to-Cycle Feedback for Combustion Control of Spark Advance at the Misfire Limit," *Journal of Engineering for Gas Turbines and Power*, vol. 140, no. 10, p. 102812, 2018.

[24] B. P. Maldonado, N. Li, I. Kolmanovsky, and A. G. Stefanopoulou, "Learning reference governor for cycle-to-cycle combustion control with misfire avoidance in spark-ignition engines at high exhaust gas recirculation–diluted conditions," *International Journal of Engine Research*, vol. 21, no. 10, pp. 1819–1834, 2020.

[25] Z. Xu, Y. Zhang, H. Di, and T. Shen, "Combustion variation control strategy with thermal efficiency optimization for lean combustion in spark-ignition engines," *Applied Energy*, vol. 251, p. 113329, 2019.

[26] C. S. Daw, M. B. Kennel, C. E. A. Finney, and F. T. Connolly, "Observing and modeling nonlinear dynamics in an internal combustion engine," *Phys. Rev. E*, vol. 57, pp. 2811–2819, Mar 1998.

[27] J. B. Heywood, *Internal Combustion Engine Fundamentals*, 2nd ed. McGraw-Hill Education, 2018.

[28] G. S. Jatana and B. C. Kaul, "Determination of SI Combustion Sensitivity to Fuel Perturbations as a Cyclic Control Input for Highly Dilute Operation," *SAE Int. J. Engines*, vol. 10, no. 3, pp. 1011–1018, 03 2017.

[29] B. P. Maldonado, B. C. Kaul, C. D. Schuman, S. R. Young, and J. P. Mitchell, "Next-Cycle Optimal Fuel Control for Cycle-to-Cycle Variability Reduction in EGR-Diluted Combustion," *IEEE Control Systems Letters*, vol. 5, no. 6, pp. 2204–2209, 2021.

[30] C. S. Daw, J. B. Green, R. M. Wagner, C. E. Finney, and F. T. Connolly, "Synchronization of combustion variations in a multicylinder spark ignition engine," *Proceedings of the Combustion Institute*, vol. 28, no. 1, pp. 1249–1255, 2000.

[31] C. Guardiola, B. Pla, P. Bares, and A. Stefanopoulou, "Cylinder charge composition observation based on in-cylinder pressure measurement," *Measurement*, vol. 131, pp. 559–568, 2019.

[32] Z. Xu and T. Shen, "Symbol-sequence statistics-based cylinder-to-cylinder variation control in spark-ignition engines," *Applied Energy*, vol. 261, p. 114406, 2020.

[33] Y. Luo, B. Maldonado, S. Liu, C. Solbrig, D. Adair, and A. Stefanopoulou, "Portable In-Cylinder Pressure Measurement and Signal Processing System for Real-Time Combustion Analysis and Engine Control," *SAE Int. J. Adv. & Curr. Prac. in Mobility*, vol. 2, no. 6, pp. 3432–3441, 2020.

[34] The Advanced Combustion and Emission Control (ACEC) Tech Team, "Advanced Combustion and Emission Control Roadmap," U.S. DRIVE Partnership, Tech. Rep., 2018.

[35] R. M. Wagner, C. S. Daw, and J. B. Green, "Low-Order Map Approximations of Lean Cyclic Dispersion in Premixed Spark Ignition Engines," in *Spring Fuels & Lubricants Meeting & Exhibition*, 2001.

[36] E. Pipitone, "A Comparison Between Combustion Phase Indicators for Optimal Spark Timing," *Journal of Engineering for Gas Turbines and Power*, vol. 130, no. 5, 2008.

[37] J. A. Caton, "Combustion phasing for maximum efficiency for conventional and high efficiency engines," *Energy Conversion and Management*, vol. 77, pp. 564 – 576, 2014.

[38] M. Bieniek, A. Stefanopoulou, J. Hoard, B. Maldonado, B. Fulton, and M. Van Nieuwstadt, "Retard to the Limit: Closed-Loop COVIMEP Control for Aggressive Exhaust Heating," *IFAC-PapersOnLine*, vol. 52, no. 5, pp. 624 – 629, 2019, 9th IFAC Symposium on Advances in Automotive Control AAC 2019.

[39] B. P. Maldonado, M. Bieniek, J. Hoard, A. G. Stefanopoulou, B. Fulton, and M. Van Nieuwstadt, "Modelling and estimation of combustion variability for fast light-off of diesel aftertreatment," *International Journal of Powertrains*, vol. 9, no. 1-2, pp. 98–121, 2020.

[40] M. Bieniek, B. Maldonado, A. G. Stefanopoulou, and J. Hoard, "Online control of process variance using feedback," in *2020 American Control Conference (ACC)*, 2020, pp. 3589–3594.

[41] A. A. Quader, "What Limits Lean Operation in Spark Ignition Engines-Flame Initiation or Propagation?" in *SAE Technical Paper 760760*. SAE International, 02 1976.

[42] B. P. Maldonado and B. C. Kaul, "Control-Oriented Modeling of Cycle-to-Cycle Combustion Variability at the Misfire Limit in SI Engines," in *Proceedings of the ASME 2020 Dynamic Systems and Control Conference*, October 2020, p. V002T26A001.

[43] P. Tunestal, "Self-tuning gross heat release computation for internal combustion engines," *Control Engineering Practice*, vol. 17, no. 4, pp. 518 – 524, 2009.

[44] B. P. Maldonado and B. C. Kaul, "Evaluation of residual gas fraction estimation methods for cycle-to-cycle combustion variability analysis and modeling," *International Journal of Engine Research*, vol. 23, no. 2, pp. 198–213, 2022.

[45] N. Ozdor, M. Dulger, and E. Sher, "Cyclic Variability in Spark Ignition Engines A Literature Survey," in *SAE Technical Paper 940987*, 03 1994.

[46] M. M. Ameen, M. Mirzaeian, F. Millo, and S. Som, "Numerical Prediction of Cyclic Variability in a Spark Ignition Engine Using a Parallel Large Eddy Simulation Approach," *Journal of Energy Resources Technology*, vol. 140, no. 5, p. 052203, 05 2018.

[47] P. R. Kumar and P. Varaiya, *Stochastic Systems: Estimation, Identification, and Adaptive Control*, ser. Classics in Applied Mathematics. Society for Industrial and Applied Mathematics, 2015.

[48] C. D. Schuman, S. R. Young, J. P. Mitchell, J. T. Johnston, D. Rose, B. P. Maldonado, and B. C. Kaul, "Low Size, Weight, and Power Neuromorphic Computing to Improve Combustion Engine Efficiency," in *2020 11th International Green and Sustainable Computing Workshops (IGSC)*, 2020, pp. 1–8.

[49] B. P. Maldonado, A. G. Stefanopoulou, and B. C. Kaul, "Chapter 8 - Artificial-intelligence-based prediction and control of combustion instabilities in spark-ignition engines," in *Artificial Intelligence and Data Driven Optimization of Internal Combustion Engines*, J. Badra, P. Pal, Y. Pei, and S. Som, Eds. Elsevier, 2022, pp. 185–212.

[50] P. J. Shayler, L. D. Winborn, M. J. Hill, and D. Eade, "The Influence of Gas/Fuel Ratio on Combustion Stability and Misfire Limits of Spark Ignition Engines," in *SAE Technical Paper 2000-01-1208*, 03 2000.

[51] K. P. Murphy, *Machine Learning: A Probabilistic Perspective*. The MIT Press, 2012.

[52] P. Hall, J. Racine, and Q. Li, "Cross-Validation and the Estimation of Conditional Probability Densities," *Journal of the American Statistical Association*, vol. 99, no. 468, pp. 1015–1026, 2004.

[53] S. Seabold and J. Perktold, "Statsmodels: Econometric and Statistical Modeling with Python," in *Proceedings of the 9th Python in Science Conference*, 2010, pp. 92 – 96.

[54] B. P. Maldonado and A. G. Stefanopoulou, "Linear Stochastic Modeling and Control of Diluted Combustion for SI Engines," *IFAC-PapersOnLine*, vol. 51, no. 31, pp. 99 – 104, 2018, 5th IFAC Conference on Engine and Powertrain Control, Simulation and Modeling E-COSM 2018.

[55] J. B. Vance, B. C. Kaul, S. Jagannathan, and J. A. Drallmeier, "Output Feedback Controller for Operation of Spark Ignition Engines at Lean Conditions Using Neural Networks," *IEEE Transactions on Control Systems Technology*, vol. 16, no. 2, pp. 214–228, 2008.

[56] A. Singh, J. B. Vance, B. Kaul, J. Drallmeier, and S. Jagannathan, "Neural Network Control of Spark Ignition Engines with High EGR Levels," in *The 2006 IEEE International Joint Conference on Neural Network Proceedings*, 2006, pp. 4978–4985.

[57] J. B. Vance, A. Singh, B. C. Kaul, S. Jagannathan, and J. A. Drallmeier, "Neural Network Controller Development and Implementation for Spark Ignition Engines With High EGR Levels," *IEEE Transactions on Neural Networks*, vol. 18, no. 4, pp. 1083–1100, 2007.

[58] J. Vance, B. Kaul, S. Jagannathan, and J. Drallmeier, "Neuro emission controller for minimising cyclic dispersion in spark ignition engines with EGR levels," *International Journal of General Systems*, vol. 38, no. 1, pp. 45–72, 2009.

[59] B. P. Maldonado, B. C. Kaul, C. D. Schuman, S. R. Young, and J. P. Mitchell, "Dilute Combustion Control Using Spiking Neural Networks," in *SAE Technical Paper 2021-01-0534*. SAE International, 2021.